



OZONE DISTRIBUTIONS OVER THE LOS ANGELES BASIN: THREE-DIMENSIONAL SIMULATIONS WITH THE SMOG MODEL

RONG LU and RICHARD P. TURCO

Department of Atmospheric Science, University of California, Los Angeles, CA 90095-1565, U.S.A.

(First received 14 September 1995 and in final form 2 May 1996)

Abstract—The UCLA Surface Meteorology and Ozone Generation (SMOG) model has been applied to simulate and analyze the distributions of ozone in the Los Angeles basin on 27 and 28 August 1987, during the Southern California Air Quality Study (SCAQS). SMOG is an integrated air pollution modeling system that includes the coupled effects of meteorology, pollutant sources and dispersion, photochemistry and aerosol microphysics, and radiative processes. High surface ozone concentrations are predicted along the slopes of the surrounding mountain barriers and in the eastern basin, as observed. The pattern of surface ozone concentrations is shown to be influenced by the evolution of oxidants within the temperature inversion that typically blankets the Los Angeles basin. In the past, dense layers of ozone have been observed to be embedded within the temperature inversion, but their origin has remained unexplained. The present model simulations reproduce these and other three-dimensional structures in the ozone distribution, as documented by measurements in the basin. The high concentrations of oxidants aloft are explained through a detailed dynamical/chemical mechanism. High mountains surrounding the Los Angeles basin block the dispersion of ozone and other pollutants and generally contain them within the basin. At the same time, vertical circulations associated with the interaction of the sea-breeze and mountain slope winds inject pollutants into the base of the inversion and create high concentrations of ozone. PAN, nitric acid, organic nitrates and a variety of other pollutants, including aerosols. The contrast between ozone concentrations at the surface and in these elevated layers can be enhanced in the evening by NO emissions, which titrate ozone near the surface. The elevated layers act as a reservoir for aged pollutants, which can be mixed downward on subsequent days to enhance surface concentrations. The recirculation of pollutants in the Los Angeles basin is thus reinforced by the presence of these oxidant layers, and may be responsible for the rapid increase in surface ozone concentrations often seen in the morning, particularly in the eastern basin where emissions of primary pollutants are relatively small. The impact on surface ozone concentrations of recirculated photochemically aged air is estimated to be as high as 8 ppbv in the eastern Los Angeles basin. These simulations represent the first quantitative description of the role of pollutants aloft on surface air quality. Copyright © 1996 Elsevier Science Ltd

Key word index: Urban air quality, photochemistry, ozone, tropospheric ozone, air pollution, Los Angeles smog, mesoscale meteorology.

1. INTRODUCTION

For more than five decades, the Los Angeles basin has suffered from severe photochemical air pollution, and remains one of the most polluted regions in the world. The photochemical smog problem in Los Angeles is associated with specific factors, including: (1) large emissions of primary pollutants such as NO_x and non-methane hydrocarbon (NMHC) within the basin; (2) ample sunlight to drive the photochemical processes that generate smog from these emissions; and (3) meteorological conditions and local topography suitable for the accumulation of air pollution. The observed distributions of pollutants in the basin include distinct elevated layers of ozone, aerosols and other compounds (e.g. Edinger *et al.*, 1972). Such distributions have been shown to result from the

interactions of coastal air flow with complex terrain (Lu and Turco, 1995). Nevertheless, the chemical composition of these layers, and the recirculation of ozone from the layers back to the surface, have never been quantitatively described.

Episodes of ozone pollution in the Los Angeles basin are usually associated with the Pacific high pressure system that controls Southern California's weather much of the year. Light synoptic winds and clear skies are typical of conditions that prevail at these times. Connected with the descending branch of the Hadley circulation, subsidence within the high pressure cell generates a strong elevated temperature inversion over the entire region. The subsidence inversion layer is present almost continuously during the summer half of the year and occurs frequently during the winter-half as well. The inversion prevents

materials emitted near the surface from being ventilated into the free troposphere, thus trapping primary and secondary air pollutants near the surface in the boundary layer. The topography of the Southern California coastal region is illustrated in Fig. 1. The Los Angeles basin is surrounded by high mountains on three sides and opens to the Pacific Ocean to the west and southwest. Because of the westerly sea breeze, this topographic configuration leads to the accumulation of airborne pollutants within the basin, particularly in the east. Topography also steers air currents that control the transport and eventual dispersion of pollutants throughout the basin (Lu and Turco, 1994). Coastal breezes and mountain winds are generated by strong daytime heating of land surfaces contrasted against the cool ocean surface nearby; these land/sea circulations play an important role in determining the transport and distribution of pollutants.

Pollutant concentrations in the Los Angeles basin vary significantly with location. Although a large fraction of the total inventory of primary pollutants is emitted in the western region of the basin, the highest surface ozone concentrations are commonly detected in the eastern basin (usually in the afternoon). Measurements of the ozone vertical concentration profile often show maximum abundances in the stable

layer above the base of the temperature inversion rather than at the surface. Observations of the vertical distributions of other pollutants, including particulates, reveal distinct elevated layers above the inversion base in both the western and eastern Los Angeles basin (Edinger *et al.*, 1972; McElroy, 1982; Smith and Edinger, 1984). By late afternoon, these layers blanket the entire western basin (Edinger, 1973; Blumenthal *et al.*, 1978), and in the evening, they extend over the eastern basin as well (Wakimoto and McElroy, 1986). Similar pollutant structures have been observed in the southern and central California coastal regions (McElroy and Smith, 1986, 1991).

The characteristics of tracer transport in the Los Angeles air-shed have been studied by Lu and Turco (1994, 1995) using a mesoscale meteorological model. In that work, a passive tracer was employed as a surrogate for secondary pollutants such as ozone, mainly to investigate their dispersion properties. It was shown that interactions between the sea breeze and mountain-induced flows control the distribution of tracer constituents over the Los Angeles basin. Pollutants found in the boundary layer in the afternoon are dispersed in three different ways: by advection through mountain passes into the high desert to the east and north of the basin; by venting into the free-troposphere above the temperature inversion layer;

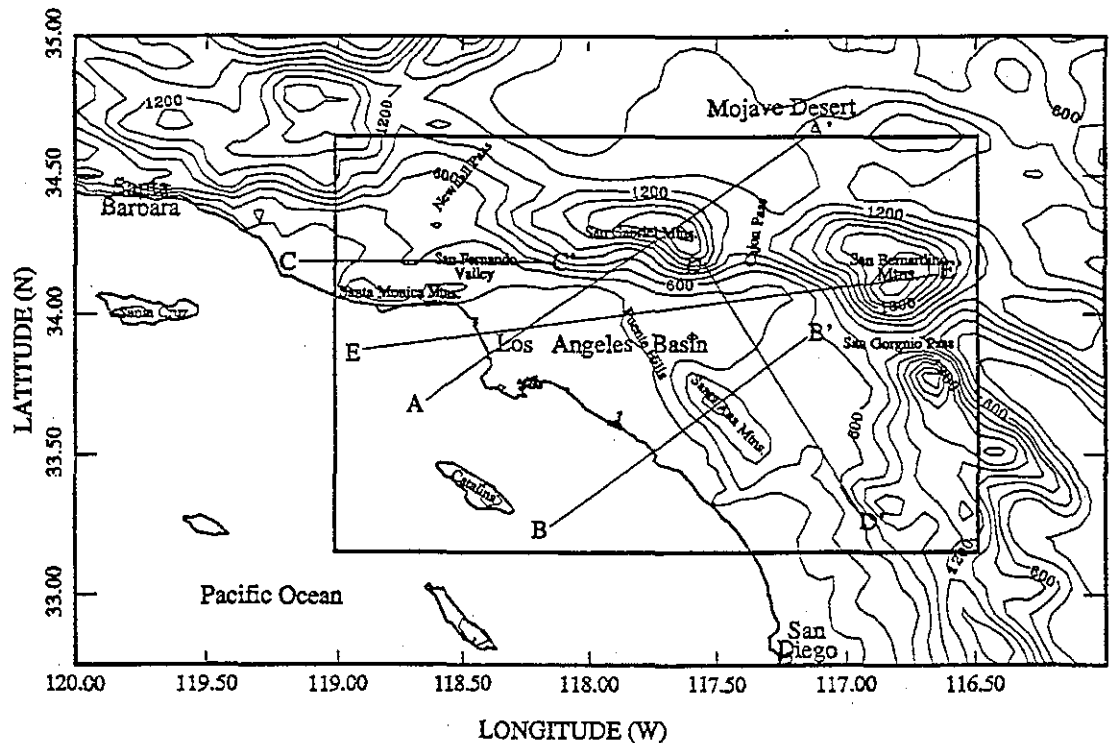


Fig. 1. The model computational domain and topography are illustrated. The larger map defines the area over which mesoscale dynamical calculations are carried out. The inner perimeter indicates the domain used for the air quality (chemistry and microphysics) simulations. Heavy solid lines indicate the coastline. Contour lines correspond to terrain elevations; the contour intervals are 200 m. The lines AA', BB', CC', DD' and EE' give the locations of the vertical cross-sections discussed in the text.

and by injection into the temperature inversion layer itself. The elevated layers of pollution mentioned above, which are seen to be embedded within the inversion layer, are themselves created by several mechanisms, including: local surface convergence forcing vertical pumping; coupled sea-breeze/mountain-slope winds that divert air into the inversion layer; and boundary layer stabilization during the early evening hours that isolates pollutants aloft. Materials trapped in the inversion layer by these mechanisms may later act as a source of oxidants for processes occurring near the surface, and may contribute to extreme ozone concentrations measured at the ground after several days of stagnant air conditions.

Because many factors influence the concentrations of ozone in the Los Angeles basin, modeling studies are needed to determine the causes of the observed ozone distribution and to evaluate its environmental impacts. Traditionally, two primary approaches to air pollution modeling have been taken. On the one hand, meteorology-based studies have emphasized the physical properties of the boundary layer and the pathways for pollutant transport over complex regional terrain (e.g. Schultz and Warner, 1982; Ulrickson and Mass, 1990b; Lu and Turco, 1994, 1995). However, such an approach is not capable of quantifying the concentrations of the most important pollutants, because chemical transformations are ignored. On the other hand, chemistry-based "air quality" models, such as the urban airshed models (McRea *et al.*, 1982 a, b; Russell *et al.*, 1988; Harley *et al.*, 1993; Scheffe and Morris, 1993), have focused on the prediction of surface concentrations of ozone (and other pollutants) using simplified representations of boundary layer physics and regional transport. Although, in this latter case, the estimated error in the predictions of hourly-averaged surface ozone concentrations often falls in an acceptable range of 35% (CARB, 1992), the "meteorological" parameters adopted in these models are represented as a number of input parameters that can be adjusted to improve the agreement with observations. In a comparison of the predicted vertical ozone profile to measurements, Roberts and Main (1992) found that the O₃ concentrations aloft from their Urban Airshed Model (UAM) simulations were under-predicted by 50–150 ppbv. The UAM predictions showed large errors in the western Los Angeles basin and offshore in the morning hours, and by midday and afternoon in the central and eastern basin as well.

Clearly, ozone concentrations are controlled both by meteorological factors that determine pollutant dispersion and by chemical transformations that generate ozone from primary pollutants. Accordingly, a coupled treatment of meteorology, tracer dispersion, and photochemistry is essential for comprehensive air quality modeling. With appropriate boundary conditions, and rigorous validation based on local observations, such a modeling system can be useful in

studying the behavior of pollution in urban airsheds throughout the world.

Lu *et al.* (1995b) applied such an air pollution model (SMOG, see below) to carry out simulations of the 27–28 August 1987 air pollution episode during the Southern California Air Quality Study (SCAQS) in the Los Angeles basin. By comparing SMOG predictions to a variety of meteorological and inert tracer observations, Lu *et al.* demonstrate that the model quite accurately represents the complex three-dimensional dispersive fields of that period. In the present work, corresponding simulations of the chemical evolution of the regional atmosphere are used to analyze the generation and dispersal of ozone and other pollutants across the Los Angeles basin. Distinct elevated layers of pollution were measured during SCAQS, and these features are reproduced in the simulations, as discussed below. Although the results presented here correspond to two specific days of the SCAQS field program, the general structure of the three-dimensional distributions of various pollutants should apply to many typical summer days in the Los Angeles basin.

In Sections 2 and 3, respectively, the elements of the SMOG modeling system, and the procedures adopted to carry out numerical simulations are outlined. Section 4 presents model predictions; first, ozone near-surface distributions are discussed in Section 4.1; next, the vertical structure of the ozone distribution in different areas of the basin is explained in Section 4.2; finally, the contrasts between the composition of polluted air aloft and near the surface are discussed in Section 4.3. In Section 5, the impact of elevated pollution layers on surface ozone concentrations in the Los Angeles basin is quantified for the first time. Section 6 summarizes our major results.

2. AN INTEGRATED MODELING SYSTEM: SMOG

A fully integrated air pollution modeling system—the Surface Meteorology and Ozone Generation (SMOG) model—has been developed specifically for studying air pollution on urban and regional scales (Lu, 1994; Lu *et al.*, 1995a; Jacobson, 1994; Jacobson *et al.*, 1995). SMOG includes detailed treatments of mesoscale meteorology, boundary layer physics, tracer advection, convection and diffusion, photochemistry, aerosol microphysics and chemistry, and solar and terrestrial radiative transfer. All of these critical processes are coupled in a single model, resulting in a powerful tool for studying the chemical origins of and control strategies for urban and regional air pollution. The performance of the SMOG model has been evaluated using field data such as that collected during the Southern California Air Quality Study (SCAQS) (Lu *et al.*, 1995b). Comparisons between simulations and observations show that the model is capable of reproducing, simultaneously, the principal features of local and regional scale

meteorology, tracer dispersion over complex terrain, and the photochemical transformations of known primary pollutants.

The mesoscale meteorological code utilized in SMOG is a three-dimensional hydrostatic primitive equation code (Lu, 1988, 1994) that predicts the dynamical and thermodynamic structure of the atmosphere—e.g. winds, turbulence, temperature, humidity and cloud fields. Previously, this model was successfully applied to forecast regional mesoscale rainfall (Lu and Cheng, 1989), as well as to investigate boundary layer behavior in a coastal region with mountainous barriers (Lu and Turco, 1994, 1995). The model incorporates physical processes such as turbulent diffusion and convective transport, water vapor condensation and precipitation, solar and infrared radiation transfer, and ground energy and water balance.

The tracer transport code that comprises the chemical, microphysical, radiative and dispersion algorithms for SMOG originated from research in the middle atmosphere and planetary atmospheres (Turco *et al.*, 1977, 1979a, b, 1982a; Toon *et al.*, 1979, 1988). Previously, the tracer code was used to carry out a number of regional and global scale simulations (e.g. Turco *et al.*, 1982b; Malone *et al.*, 1986; Toon *et al.*, 1987, 1988, 1989a; Westphal *et al.*, 1988, 1991). In the tracer code, a time splitting algorithm is used to calculate separately the effects on species concentrations of advective and diffusive transport, chemistry, and microphysics. A finite-element method is adopted for horizontal advection and a finite-difference scheme for vertical transport and diffusion. This approach leads to efficient and accurate dispersion solutions with minimal computer memory demands.

The gas-phase chemistry algorithm is based on a modified version of the carbon-bond-extended mechanism (CBM-EX) (Gery *et al.*, 1989). The photochemical scheme consists of 100 species and 223 chemical reactions and photoprocesses. The concentrations of 95 active species are predicted in each model cell. To overcome the extreme "stiffness" in the equations of chemical kinetics, solutions are obtained using an accelerated version of the well-known Gear solver (SMVGEAR) (Jacobson and Turco, 1994). The basic Gear algorithm is a multistep, variable-order predictor-corrector scheme that is known to provide robust and accurate solutions for reactive chemical systems (Gear, 1969, 1971). Compared to the original Gear code, SMVGEAR provides equivalent solutions with an increase in computational speed of a factor of 100 or more for three-dimensional problems (Jacobson and Turco, 1994).

An efficient two-stream radiative transfer model developed by Toon *et al.* (1989b) for vertically inhomogeneous multiple-scattering turbid atmospheres, is employed to calculate solar and infrared heating rates and photodissociation rates. The scattering and absorption by aerosols and clouds are computed with a fast Mie code (Toon and Ackerman, 1981). The accuracy of the radiative transfer solutions for

photodissociation rates and heating rates is typically better than 90%.

The present tracer code also includes all of the important processes that control aerosol behavior—nucleation, coagulation, condensational growth and evaporation, sedimentation, dry and wet deposition, chemical equilibrium, and aqueous chemistry (Jacobson, 1994). However, aerosol tracers are not treated in the present work.

3. SIMULATIONS FOR SCAQS

Most previous analyses of the SCAQS data and other measurements have focused on surface conditions: the general morphology of surface ozone, ground-level distributions of other pollutants including NO_x , and the dispersion of inert tracers released and measured at the ground. By contrast, the simulations performed here address the full three-dimensional distributions of ozone during the Southern California Air Quality Study (SCAQS) of 27–28 August 1987. The overall model computational domains and topographical relief for this region are illustrated in Fig. 1. The meteorological component of the SMOG model employs an 85×55 horizontal grid system with grid spacing of 0.05° longitude (4.6 km) by 0.045° latitude (5 km). The domain for the tracer chemistry simulations contains 51×34 grid cells covering the Los Angeles basin and adjacent areas nested within the meteorological domain. Twenty non-uniform vertical layers, with the highest resolution in the lower troposphere, are used for both models in the coupled system. The corresponding sigma levels are 0, 0.19, 0.342, 0.462, 0.557, 0.633, 0.693, 0.74, 0.778, 0.808, 0.831, 0.85, 0.869, 0.888, 0.906, 0.925, 0.943, 0.959, 0.974, 0.988, and 1.

In the present simulations, boundary layer fluxes of sensible and latent heat and water vapor are calculated using a multi-layer hybrid boundary layer model (Lu and Turco, 1994). A 10-layer soil model is included in the computation of the surface fluxes. The thickness of the soil layers are 0.005, 0.008, 0.013, 0.021, 0.034, 0.056, 0.090, 0.146, 0.237, and 0.390 m, respectively, from the surface to a depth of 1 m. The surface and soil parameters can be variable, but were assumed to be uniform over land surfaces in the present simulation (refer to Table 1 for the adopted parameters). Initially, the soil temperature is the same as the initial surface temperature to a depth of 1 m, and the soil moisture content is $0.16 \text{ m}^3 \text{ per m}^3$ to that depth.

The meteorological model is initialized each day at 4:00 a.m. PST and run for 24 h. Upper air soundings taken around 4:00 PST are used to interpolate the initial meteorological conditions over the entire regional grid. First, the meteorological data are analyzed on horizontal surfaces. The wind components, temperature, and relative humidity are interpolated to the horizontal grid points specified in the model

Table 1. Surface and soil parameters used in the model simulations

Surface roughness over land (z_0)	0.75 m
Surface roughness over ocean (z_0)	0.001 m
Surface albedo (A)	0.2
Sea surface temperature (T_{ss})	16°C
Surface emissivity (ϵ_s)	0.95
Soil saturated moisture content (W_{sat})	0.435 m ³ per m ³
Soil saturated moisture potential (Ψ_{sat})	- 0.218 m
Soil saturated hydraulic conductivity (K_{sat})	3.41×10^{-5} m s ⁻¹
Dimensionless exponent for soil (b)	4.90
Volumetric heat capacity for dry soil ($\rho_s c_s$)	1.34×10^6 J m ⁻³ K ⁻¹
Volumetric heat capacity for water ($\rho_w c_w$)	4.186×10^6 J m ⁻³ K ⁻¹

domain, using a weighting function that varies as the inverse square of the distance between the station point and the grid point. The weighting function is further adjusted according to the maximum height of the terrain between the station point and the grid point; hence, the presence of topographical barriers are recognized in the scheme to reduce the influence of measurements at stations lying on the far side of a mountain range. Finally, the analyzed fields on horizontal surfaces are interpolated onto the model σ layers using a cubic spline method. In this study, meteorological data measured at surface stations have not been used in the analysis of model initial conditions.

The lateral boundary conditions for the meteorological model are open boundaries (Lu, 1994). To include the effects of larger scale forcing, the model predictions are nudged toward prescribed (observed large-scale) values in a narrow zone along each lateral boundary. The boundary zone has a thickness of three grid intervals. The prescribed boundary parameter values are the initial values interpolated within the boundary zone. The geostrophic winds in the simulation are the winds at 4:00 a.m. PST averaged over all stations in the region. Neither the prescribed boundary values nor the geostrophic winds are changed during a 24 h simulation period. Therefore, the synoptic conditions in the early morning hours has been assumed to be representative for that day. For the chemical tracers in the SMOG model, constant inflow and open outflow boundary conditions are adopted, consistent with the boundary velocity fields determined above. To calculate the tracer inflow fluxes, the background concentrations given in Table 2 are assumed.

The air quality simulations described here begin at 4:00 PST on 26 August 1987 and continue for three days until 4:00 PST on 29 August. During this three-day period, the meteorological fields were re-initialized once each day at 4:00 PST (i.e. on 27 and 28 August). To initialize the three-dimensional distributions of the principal chemical tracers, surface concentrations of O₃, NO, NO₂, CO, SO₂, and non-methane hydrocarbons (NMHCs) were interpolated onto the SMOG grid from surface measurements over the SCAQMD network at 4:00 PST on 26 August. Since

Table 2. The gas-phase species concentrations used for background values and lateral boundary conditions in the simulations

Species name	Concentrations (ppbv)
CO	110
NO	0.01
NO ₂	1
HONO	0.01
O ₃	40
CH ₃ CO ₂ NO ₂	0.05
HCHO	1
C ₂ H ₄	1
PAR	10
OLE	0.1
ALD2	3
TOL	1.1
XYL	0.6
CH ₃ OH	0.1
CH ₃ CH ₂ OH	0.01
ISOP	0.01
CH ₄	1650

only three NMHC measurements are available for this time, NMHC concentrations at other station points were estimated from NO_x concentrations under the assumption that the NMHC to NO_x concentration ratio is 8.8 mole C per mole-NO_x in early morning ambient air (Fujita *et al.*, 1990). The interpolated surface tracer concentrations were then extrapolated from the surface upward to 970 mb (about 350 m above the sea level) to represent ambient concentrations beneath the pre-existing temperature inversion. These initial conditions, particularly above the surface, are quite uncertain. In fact, as this study later emphasizes, high concentrations of ozone and other compounds are usually found in distinct layers above the surface in the morning hours. Our simulations show, however, that the initial conditions only significantly influence the model results during the first day. Accordingly, our analysis focuses on the predictions from the second and third days of the simulation period.

The initialization of the highly reactive tracers in the SMOG chemistry occurs automatically as the model is spun-up during the first morning when the photochemical processes that provide sources of radicals are activated.

The dynamical and chemical evolution of the tracer distributions depends critically on the continuing emissions of primary pollutants over the study period. In the present work, the California Air Resources Board (CARB) emission inventory for 26–28 August 1987 was utilized (Allen and Wagner, 1992). For gaseous species, the emission inventory provides gridded hourly emission rates of CO, NO_x (NO, NO₂ and HONO), SO_x (SO₂ and SO₃), and reactive organic gases (ROGs) for both distributed surface and point stack emissions. However, it has been found that the ROGs and CO emissions are significantly underestimated in this inventory (e.g. Ingalls *et al.*, 1989; Pierson *et al.*, 1992; Fujita *et al.*, 1992), which can lead to serious under-prediction of ozone concentrations in the Los Angeles basin (Harley *et al.*, 1993; Jacobson *et al.*, 1995). Fujita *et al.* (1992) compared the ratios of CO and NMHCs to NO_x in the emission inventory and in ambient air in the Los Angeles basin. The ambient CO/NO_x and NMHC/NO_x ratios in the early morning are about 1.5 and 2–2.5 times, respectively, higher than the corresponding ratios in the emission inventory. It is reasonable to assume that the NO_x emissions in the inventory are fairly accurate; moreover, measured ambient concentration ratios, particularly for CO/NO_x and NMHC/NO_x in the morning, approximately represent the actual ratios in emissions. Accordingly, the CO and NMHC emissions in the CARB inventory may be corrected using appropriately measured concentration ratios. In this study, the emissions are adjusted upward based on ambient NMHC/NO_x ratios reported by Fujita *et al.* (1992) for the SCAQS period (Lu, 1994; Lu *et al.*, 1995b). In this case, the mobile hot-exhaust emissions of organic gases are increased by a factor of 3 and the total CO emission is increased by a factor of 1.6. Further, the total emissions of organic gases are scaled by a second factor to bring the ratio of NMHC/NO_x in the total daily inventory integrated over the entire Los Angeles domain to a value of 8.8 mole C per mole-NO_x (Fujita *et al.*, 1990). Obviously, this adjusted emission profile represents a first approximation, until precise analysis can reduce the uncertainties in emissions.

4. SIMULATED OZONE DISTRIBUTIONS

Three-dimensional ozone distributions over the Los Angeles basin were simulated for the period from 4:00 PST 26 August to 4:00 PST 29 August 1987. The results for 27 August are discussed in this section inasmuch as the predicted ozone distributions are very similar on 27 and 28 August.

4.1. Surface ozone distributions

Figure 2a–c shows the predicted distributions of ozone in the surface layer of the SMOG model for 27 August 1987 at 10:00, 14:00 and 18:00 PST. In the

Los Angeles basin, a large portion of NMHC and NO_x are emitted in the western region of the basin (Los Angeles County). However, throughout the day ozone concentrations in the eastern basin, in the San Fernando valley and near high mountains are much higher than those in the western basin. Analysis of three-dimensional ozone distributions in the basin can yield a better understanding of the evolution of surface ozone concentrations.

In the early morning, surface ozone abundances lie below 1 pphmv (part-per-hundred-million by volume) everywhere in the basin except on some mountain slopes and near the coast. The low concentrations of O₃ near the surface are caused in part by NO titration in the stable boundary layer at night. After sunrise, ozone concentrations increase over the entire basin. In the early morning hours, light winds within the boundary layer are not effective in dispersing emitted pollutants from their source regions. However, by 10:00 PST, as the mixed layer begins to deepen, ozone concentrations rise to 8 pphmv and above in the eastern basin and in the San Fernando valley, where emissions of primary pollutants remain relatively small. In these regions, our simulations suggest that rapid increases in ozone surface concentrations are related to downward mixing of aged polluted air aloft (see Section 5).

As the sea breeze develops later in the day, pollutants are carried inland from the western basin toward the east and up the mountain slopes. At the same time, ozone is copiously generated by photochemical processes driven by NO_x and NMHC emissions. A sharp gradient in the ozone concentration from the coastal region toward the inland mountains is evident by the afternoon (Fig. 2b). The regional mountains act as a barrier, confining polluted air within the extended coastal plain. Because of the strengthening sea breeze, the largest ozone concentrations develop in the eastern basin and San Fernando valley and along the southern slopes of the San Gabriel Mountains (in the San Gabriel valley).

The photochemical generation of ozone diminishes in the late afternoon. During the early evening, on-shore breezes sweep the western basin clean (Fig. 2c). Moreover, continuing surface emissions of NO_x titrate ozone near the ground (producing nitrogen dioxide), thus further reducing local ozone densities. Accordingly, the maximum ozone concentrations drift toward the slopes of the surrounding mountains. Throughout the afternoon and evening, polluted air is transported upslope through mountain passes into the desert regions beyond, while some is vented into the free troposphere. Later at night, ozone concentrations near the surface are low throughout the coastal basin. However, along the mountain slopes, high ozone concentrations can still be found, which are related to the elevated layers of pollution formed over the basin during the afternoon and stabilized in the thermal inversion layer at night.

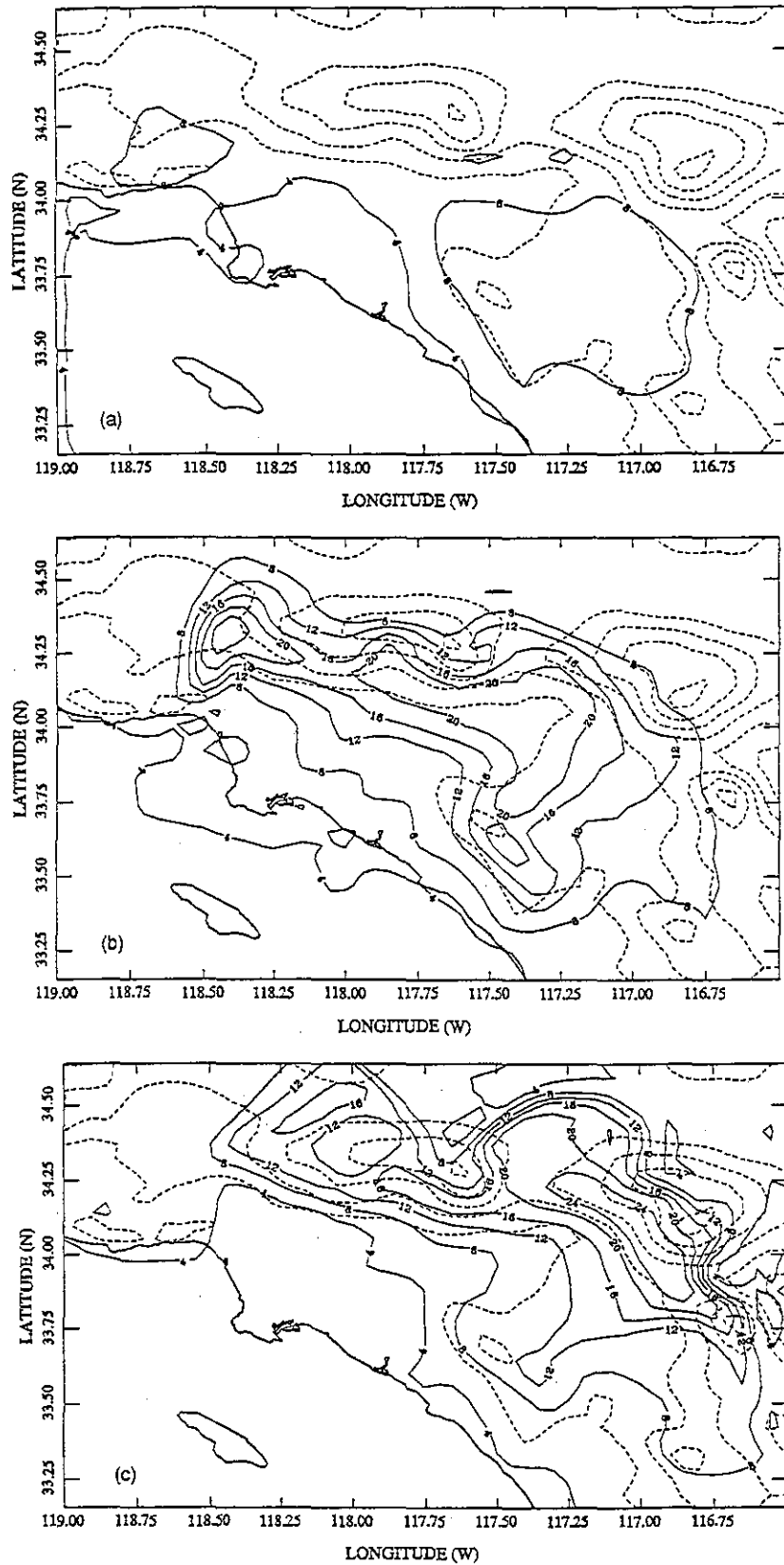


Fig. 2. Simulated distribution of ozone near the surface on 27 August 1987 (solid contours). The ozone contour intervals are 4 ppmv. Dashed lines indicate terrain elevation with a contour interval of 400 m. (a) 10:00 PST; (b) 14:00 PST; (c) 18:00 PST.

4.2. Vertical ozone distributions and elevated pollution layers

Surface ozone concentrations are, of course, merely the lower boundary values of the full three-dimensional ozone distribution. Figure 3 illustrates several predicted and measured vertical ozone profiles for 27

August 1987. The measurements were taken from an aircraft platform during the Southern California Air Quality Study (SCAQS), in which spiral patterns were flown to obtain vertical profiles (Anderson *et al.*, 1989). The SMOG model results correspond to ozone profiles at grid points closest to the aircraft sampling

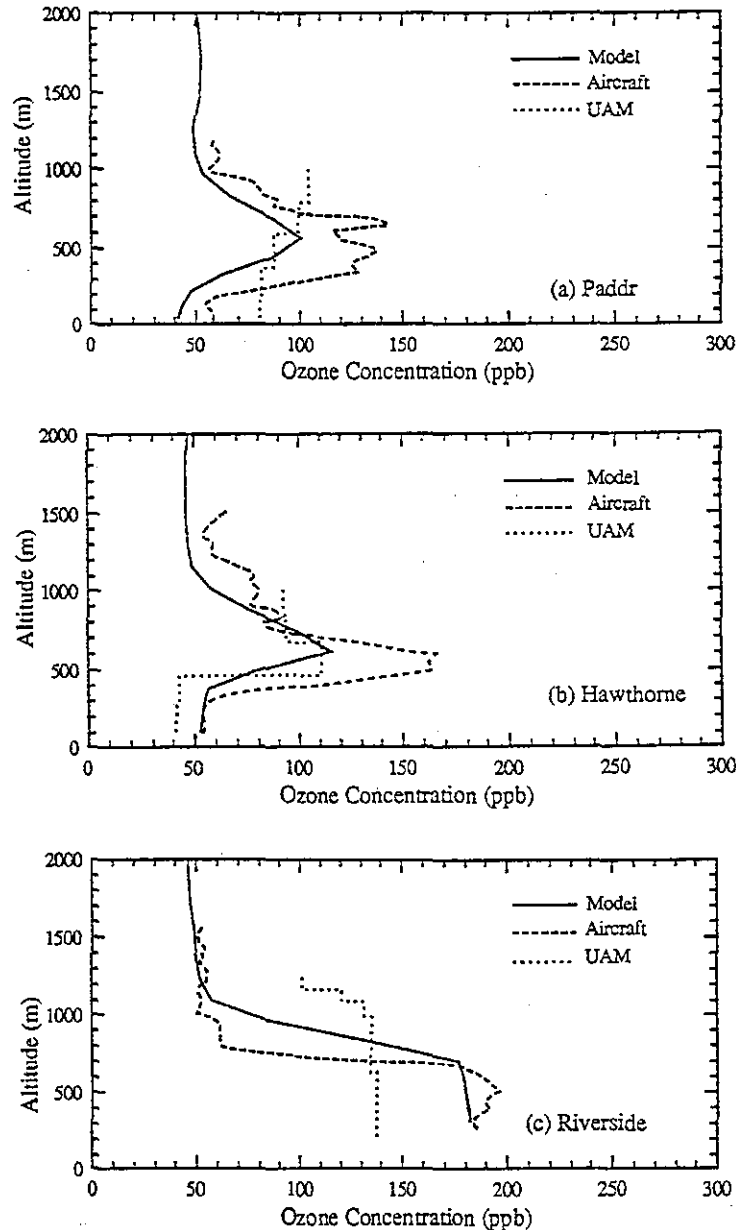


Fig. 3. Comparison of measured and predicted vertical profiles of ozone on 27 August 1987. Solid lines represent the SMOG model predictions carried out for this study. Dashed lines represent aircraft measurements, while the dotted lines are predictions from the Urban Airshed Model (UAM). The aircraft data and UAM predictions were obtained from Roberts and Main (1992). The comparisons are for: (a) a location 15 km south of Long Beach over water, where the measurements were taken from 11:24 to 11:30 PST, the SMOG model results are at 12:00 PST, and the UAM predictions represent an average for the period 11:00–12:00 PST; (b) Hawthorne, with measurements from 11:08 to 11:15, SMOG at 11:00, and UAM from 11:00 to 12:00; (c) Riverside, with measurements from 11:58 to 12:05, SMOG at 12:00, and UAM from 12:00 to 13:00; (d) Cable Airport, with measurements from 13:59 to 14:05, SMOG at 14:00, and UAM from 14:00 to 15:00.

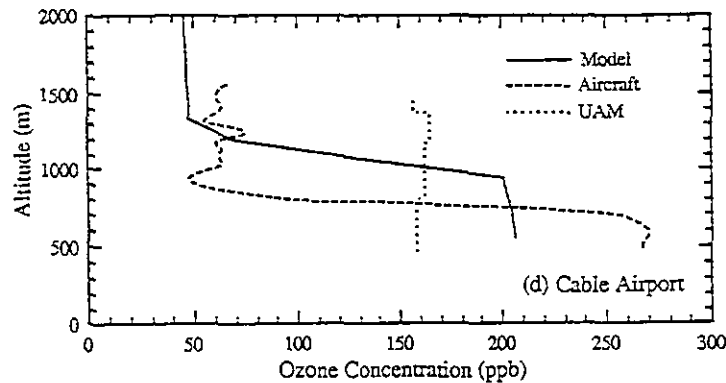


Fig. 3d.

sites in space and time. Figure 3 also displays model simulations carried out for the final Air Quality Management Plan (AQMP) using the Urban Airshed Model (UAM) (SCAQMD, 1990, 1991; Roberts and Main, 1992). In the UAM simulation, wind fields were obtained from the Colorado State University Mesoscale Model (Ulrickson and Mass, 1990a) with subsequent post-processing for use in UAM. The mixing height fields were calculated by the Holzworth method (Cassmassi and Durkee, 1990), which is based on upper-air temperature sounding data and surface temperature measurements. The emission inventory used in the UAM predictions is similar to the CARB inventory, but without adjustments. Wagner *et al.* (1992) found that the under-prediction of surface ozone concentrations by UAM could be compensated by adjusting the ROG emissions upward relative to the CARB inventory. In this study, however, we focus on the vertical structure of the ozone distribution.

Vertical ozone profiles at midday in the western Los Angeles basin at the sites designated "Paddr" (a flight path intersection over the ocean 15 km south of Long Beach) and "Hawthorne" are shown in Fig. 3a and b. The measured ozone concentrations near the surface and above 1000 m are around 50–60 ppbv at both sites. Very high ozone concentrations of 120–150 ppbv were detected between 300 and 700 m at Paddr, and more than 160 ppbv between 500 and 600 m at Hawthorne. Similar vertical structures are predicted by the SMOG model (Fig. 3), although the maximum ozone concentrations in these layers are 40–50 ppbv lower than measured values. This observed stratified vertical structure is suggested in the UAM simulation for Hawthorne, but not for Paddr.

At two sites in the eastern Los Angeles basin, high ozone concentrations were measured in the mixed layer at midday and in the afternoon (Fig. 3c and d, respectively). Above the top of the mixed layer, ozone concentrations decreased sharply to about 60 ppbv at both sites. SMOG reproduces the observed vertical ozone profile at Riverside quite accurately. At Cable Airport, which is located on the steep southern slopes of the San Gabriel mountains, the predicted

mixed-layer ozone abundance is about 20% lower than the measurements. This under-prediction is apparently related to the over-prediction of the mixed layer depth at this site. At both sites, the upper-level ozone concentrations are also accurately simulated in the SMOG model. By contrast, the UAM model fails to predict the vertical structure at either of these sites, which might be a result of the meteorological data used to force the model, or the coarser vertical resolution in that model. Neither surface nor upper-level ozone abundances are correctly forecast by UAM.

The full picture of ozone and other pollutant distributions in a complex geographical setting such as Los Angeles basin cannot be obtained from a limited number of aircraft sampling flights. Hence, simulations with a comprehensive air quality modeling system like SMOG can more clearly delineate the evolution and patterns of regional pollution. Lu and Turco (1995) investigated the characteristics of inert-tracer transport in the Los Angeles area and quantified the mechanisms that lead to the formation of contaminated layers over the basin. In the present work, the explicit inclusion of chemical processes leads to the prediction of distinct ozone layers—through similar dynamical mechanisms—as have been observed. The impact of these polluted layers on surface conditions is quantified in Section 5. In the following subsections, the vertical and horizontal structure of these ozone distributions are described.

4.2.1. Layers covering the western coastal regions. Ozone concentrations projected onto a vertical plane bisecting the Los Angeles basin from Santa Monica Bay to the San Gabriel Mountains (path AA' in Fig. 1) are illustrated at two times of the day in Fig. 4a and b. In the morning hours, residual layers of ozone created the previous day are seen at an altitude of about 700 m (Fig. 4a). These layers are embedded within the stabilized temperature inversion blanketing the region at this time; hence, they are effectively decoupled from the surface. Such layers were originally created over the coastal regions during the afternoon hours (Fig. 4b) through the intrusion of

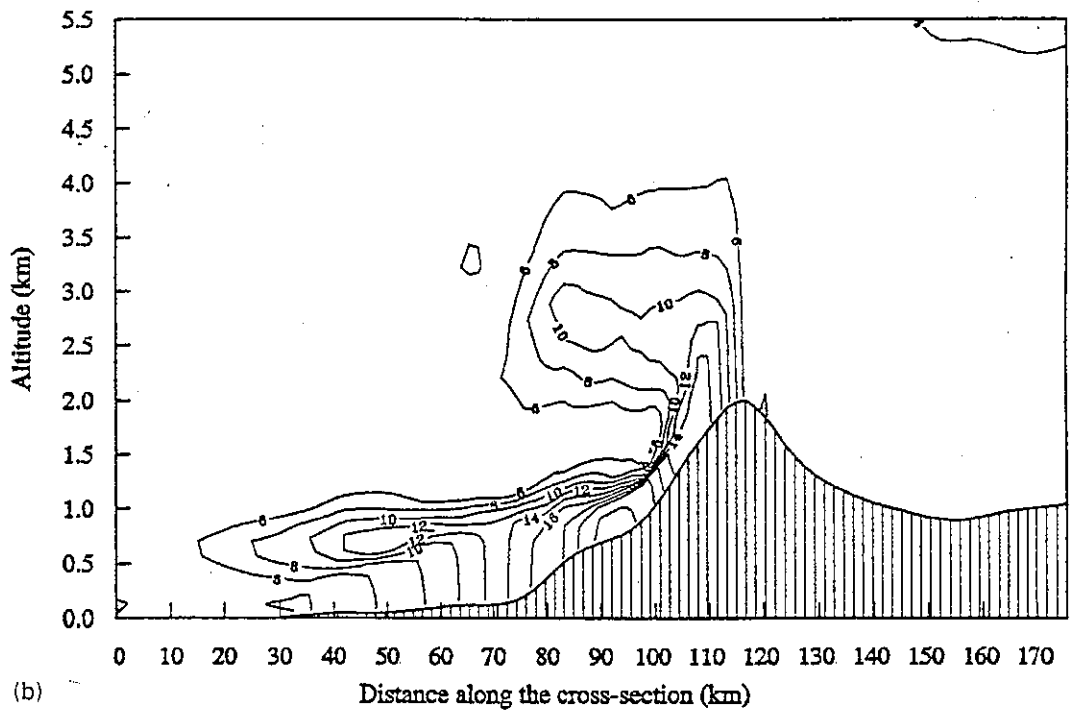
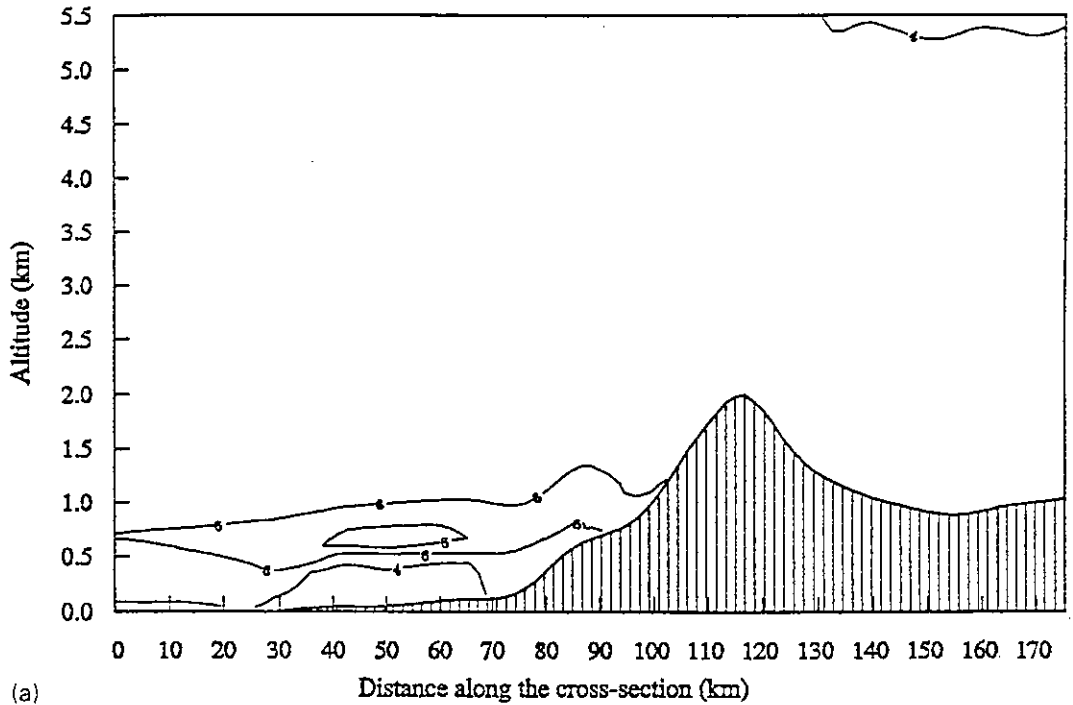


Fig. 4. Calculated ozone concentrations (contours, in intervals of 2 pphmv) for a vertical cross-section that extends from Santa Monica Bay to the San Gabriel Mountains (AA' in Fig. 1) on 27 August 1987. The topography is highlighted by striping. (a) 10:00 PST; (b) 14:00 PST.

sea breezes onto the coastal plain (Lu and Turco, 1995). As a result, a dense ozone layer is created at about 800 m by 14:00 PST (Fig. 4b), covering most part of the western basin.

Over the coastal plain, nitric oxide emitted into the boundary layer partially titrates ozone near the surface (by the reaction, $\text{NO} + \text{O}_3 \rightarrow \text{NO}_2 + \text{O}_2$), leaving the ozone aloft unaffected. Therefore, surface

ozone concentration is relatively low over the western coastal region. This mechanism can enhance the layered structure, however, is not responsible for the layered structure. To see this, the concentrations of "total oxidants" (that is, $O_3 + NO_2$) on the cross section AA' are illustrated in Fig. 5 (compare this to Fig. 4b). A similar "plume" signature is noted in the distribution of total oxidants, indicating that titration alone cannot explain the vertical structure observed for ozone. Titration by NO may intensify the existing vertical structure, however.

Similar pollution layers are predicted for 28 August 1987 as well (Fig. 6). In this instance, high ozone concentrations extend far westward over the ocean by 16:00 PST. In fact, most of the time during the two days of this simulated event, ozone achieved maximum concentrations in these elevated layers.

4.2.2. Layers injected into the free troposphere. Another important feature of the ozone distributions in Figs 4–6 is the presence of distinct layers of ozone in the free troposphere above the mountain ridge line. Normally, the strong temperature inversion blanketing the Los Angeles basin would prevent boundary layer pollutants from entering the free atmosphere. However, forced by intense solar heating, upslope mountain thermal winds create a chimney effect that injects pollutants directly into the free troposphere (Lu and Turco, 1995). In Figs 4–6, the ventilating effect of the San Gabriel mountains results in the formation of ozone plumes between roughly 2–5 km

altitude over the Los Angeles basin (also see many of the figures following). This mountain venting is an important sink for pollutants within the Los Angeles basin. Importantly, these contaminated plumes injected into the free troposphere contribute to the long-range effects of Los Angeles air pollution.

4.2.3. Layers created by near-coastal mountains. Lu and Turco (1995) found that the combined sea breeze and mountain flow circulation associated with terrain adjacent to the coastline can produce extensive layers of pollution offshore above the ocean surface. Induced sea breezes carry relatively clean air onshore. At the same time, air flowing up warm mountain slopes circulates pollutants from the boundary layer into the capping inversion layer and transports the pollutants offshore in a re-circulation pattern. Figure 7 gives predicted ozone distributions on a vertical cross-section bisecting the coastal Santa Ana mountains (path BB' in Fig. 1) at 14:00 PST. The layer of pollution, generated by vertical motions, extends from the western slopes of the mountains far offshore. The layer contains not only ozone, but other secondary and primary pollutants such as nitric acid (HNO_3), peroxyacetyl nitrate (PAN), organic nitrates and carbon monoxide. Thus, as an example, the carbon monoxide distribution is illustrated in Fig. 8.

4.2.4. Layers associated with surface convergence zones. In regions where surface air currents converge, pollutants can be efficiently lifted from the boundary layer into the inversion layer and free troposphere.

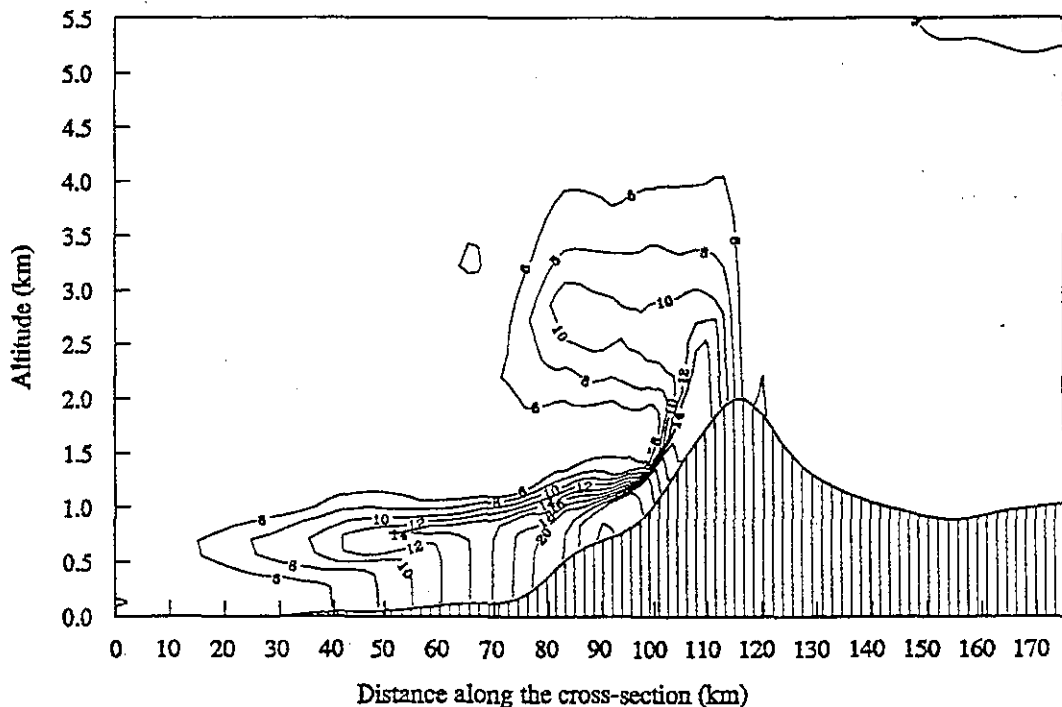


Fig. 5. Predicted "total" oxidant ($O_3 + NO_2$) concentrations (contours, in intervals of 2 pphmv) for vertical cross section AA' (Fig. 1) from Santa Monica Bay to the San Gabriel Mountains at 14:00 PST on 27 August 1987.

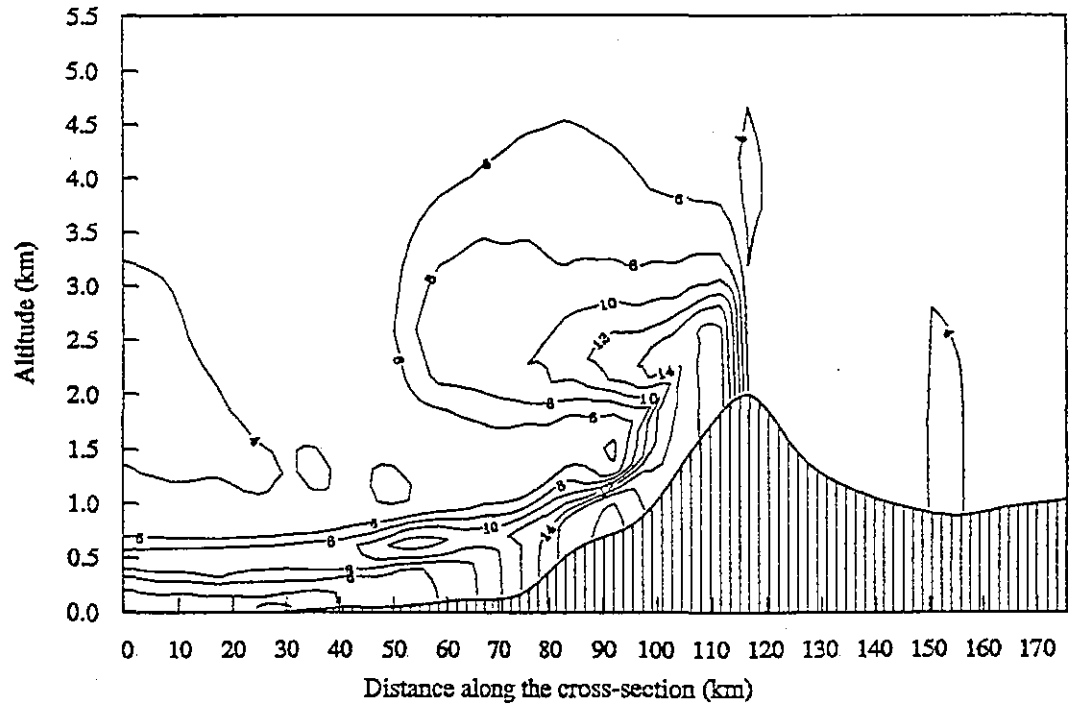


Fig. 6. Simulated ozone concentrations (contours, in intervals of 2 ppbmv) for vertical cross-section AA' (Fig. 1) extending from Santa Monica Bay to the San Gabriel Mountains at 16:00 PST on 28 August 1987.

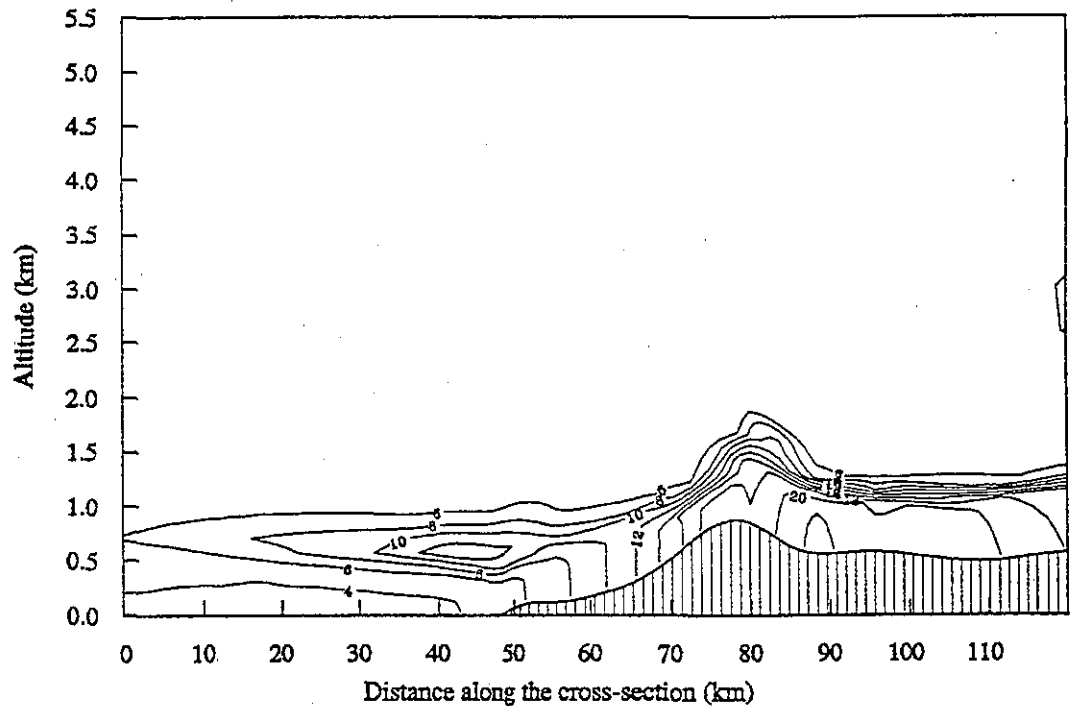


Fig. 7. Calculated ozone concentrations (contours, in intervals of 2 ppbmv) for vertical cross-section BB' (Fig. 1) bisecting the Santa Ana Mountains, at 14:00 PST on 27 August 1987.

Dense layers of pollution are commonly observed near such convergence zones (e.g. Smith and Edinger, 1984). Figure 9 shows the ozone distributions (on a vertical cross-section following path CC' in Fig. 1) in

the vicinity of the San Fernando Valley where easterly and westerly sea breezes converge. Polluted air from the Los Angeles basin is transported to the convergence by thermally-induced easterly flow, is lofted

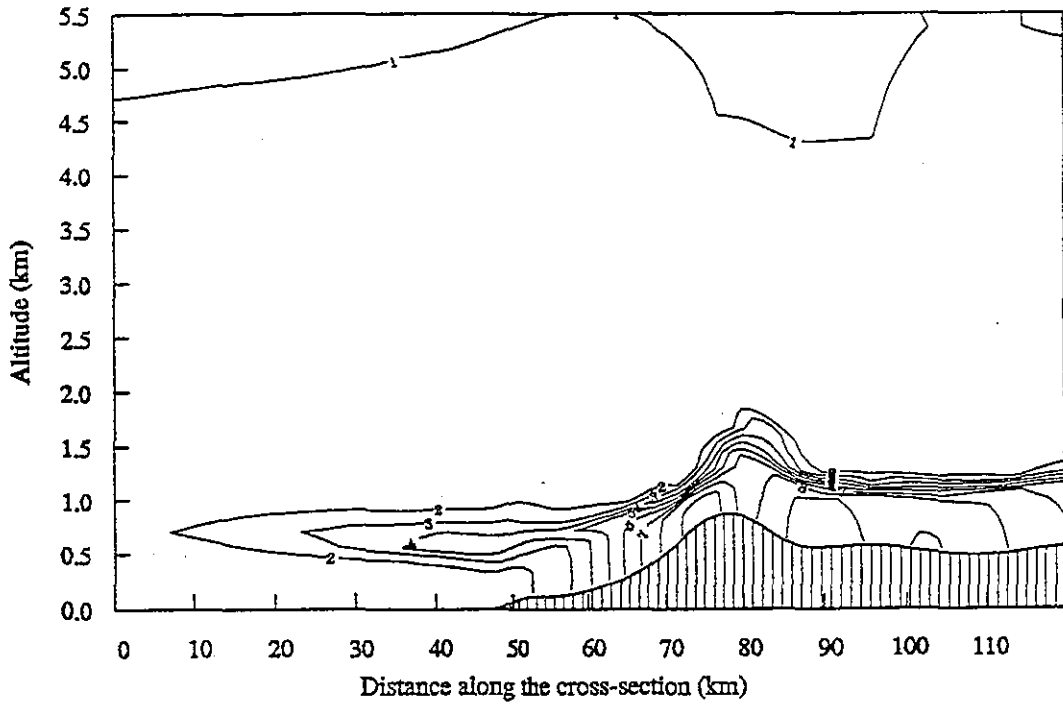


Fig. 8. Predicted CO concentrations (contours, in intervals of 0.1 ppmv) for vertical cross-section BB' (Fig. 1) bisecting the Santa Ana Mountains, at 14:00 PST on 27 August 1987.

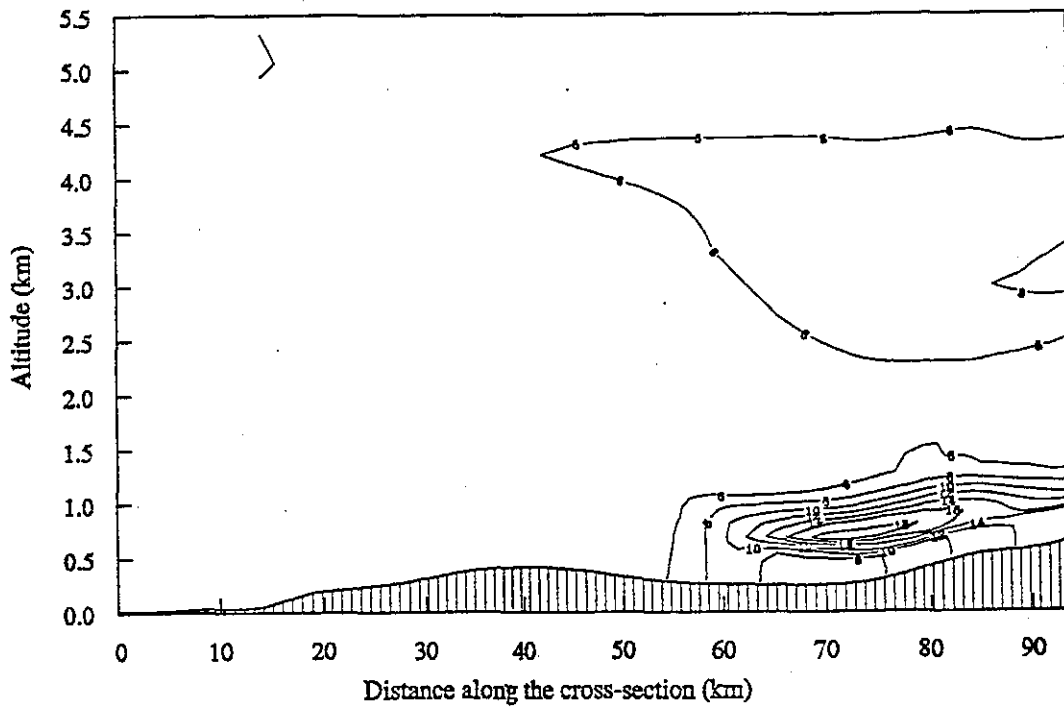


Fig. 9. Simulated ozone concentrations (contours, in intervals of 2 ppmv) for vertical cross-section CC' (Fig. 1) through the San Fernando convergence zone at 14:00 PST on 27 August 1987.

owing to the convergence, and is then carried back in the westerly return circulation. Accordingly, a layer of ozone is formed aloft to the east of the surface convergence.

Another prominent surface convergence occurs near Lake Elsinore, as illustrated in Fig. 10 (refer to path DD' in Fig. 1). At 16:00 PST, a plume with a peak ozone concentration of 21.5 ppmv is situated

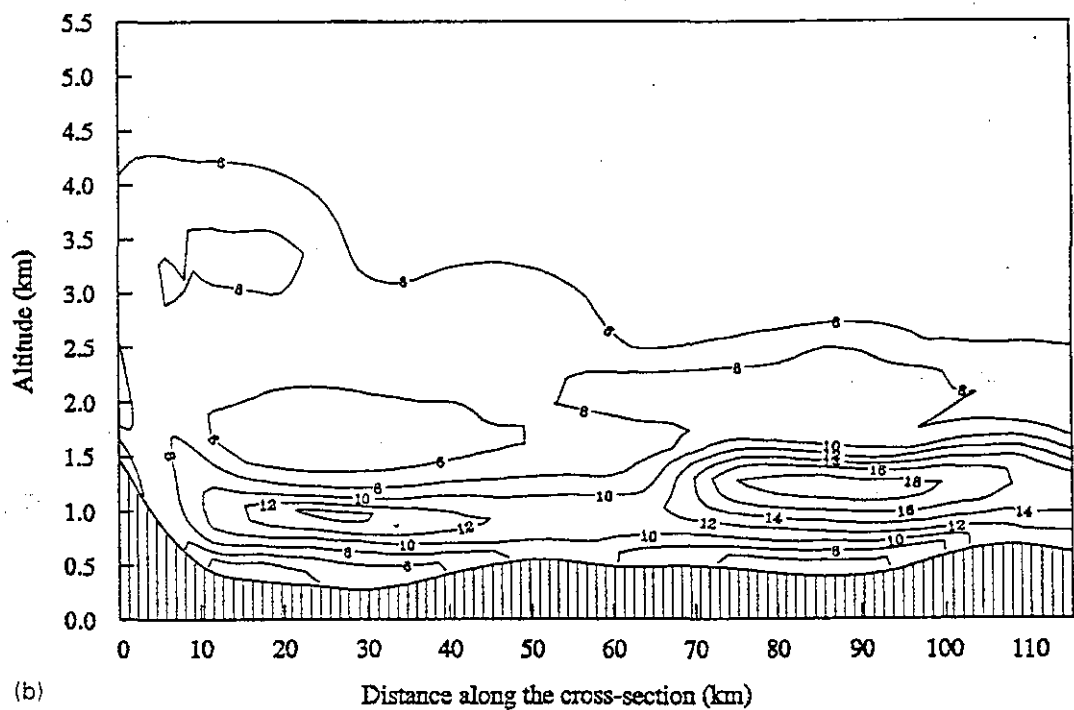
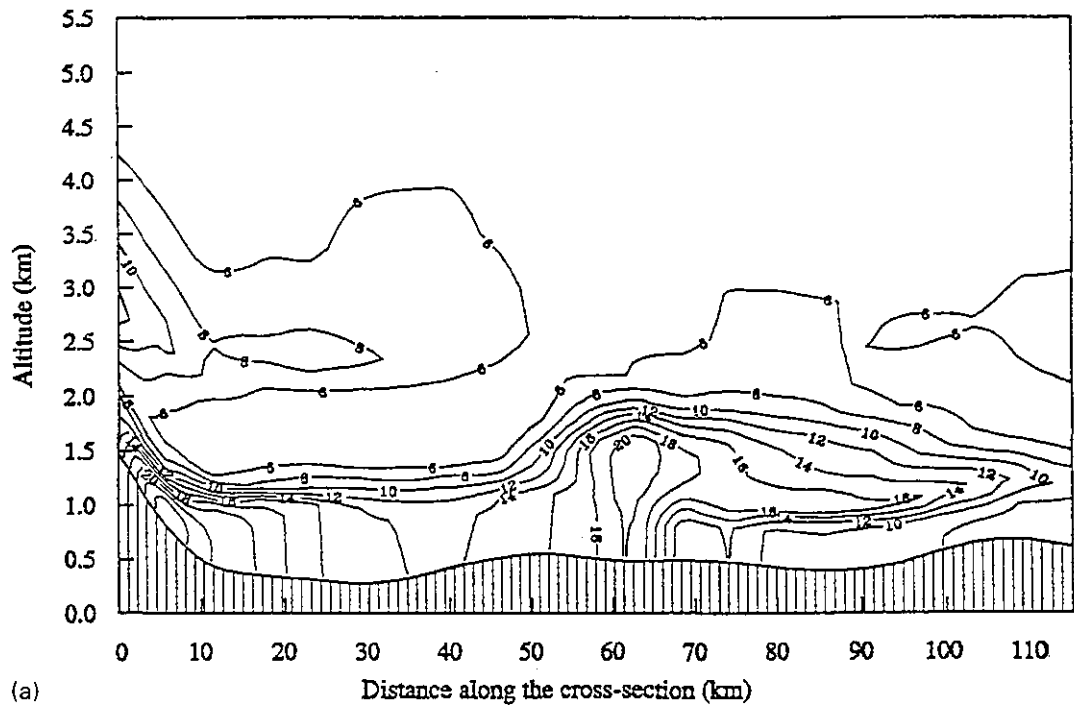


Fig. 10. Calculated ozone concentrations (contours, in intervals of 2 pphmv) for vertical cross-section DD' (Fig. 1) bisecting the Elsinore convergence zone, on 27 August 1987. (a) 16:00 PST; (b) 20:00 PST.

above the surface convergence. This plume extends southward from the convergence at an altitude of ~ 1 km for a distance of 50 km. By 20:00 PST, layers of high ozone concentration blanket the entire region. However, the ozone layers to the north (lying in the

eastern Los Angeles basin) are caused by processes described in Section 4.2.5 below.

4.2.5. *Layers in the eastern Los Angeles basin.* The evolution of ozone distributions across the entire Los Angeles basin, extending from the coastal region to

the eastern mountain barrier, is depicted for 27 August in Fig. 11 (the ozone concentrations are displayed on a vertical plane extending from Santa Monica Bay to the San Bernardino Mountains). By 12:00 PST (Fig. 11a), ozone concentrations at the surface show a systematic increase from the western coast toward the eastern mountains. The coastal zone lies beneath a distinct layer of ozone situated at about 600 m (also refer to Section 4.2.1). In the eastern basin, on the other hand, ozone is confined to the mixed layer in modest abundances. During the afternoon, sea breezes transport pollutants within the boundary layer from source regions in the western basin to regions of accumulation in the eastern basin. Ozone is continuously produced from primary pollutants over this period. By 16:00 PST, very high ozone concentra-

tions are found at the surface in the eastern regions of the Los Angeles basin, and mountain venting is forcing ozone into the free troposphere. In the early evening hours (Fig. 11c), the boundary layer has stabilized and photochemically-aged air is inserted into the temperature inversion (Lu and Turco, 1994, 1995). Cooler marine air moves inland undercutting the warmer mixed-layer air, further emphasizing the contrast between ozone concentrations at the surface and aloft. Consequently, the entire basin is soon blanketed by ozone layers (Fig. 11c). These ozone layers remain over the basin during the night. Similar behavior was seen in the SMOG simulations for 28 August (Fig. 12).

Implications. Human health and environmental impacts of exposure to ozone are directly related to its

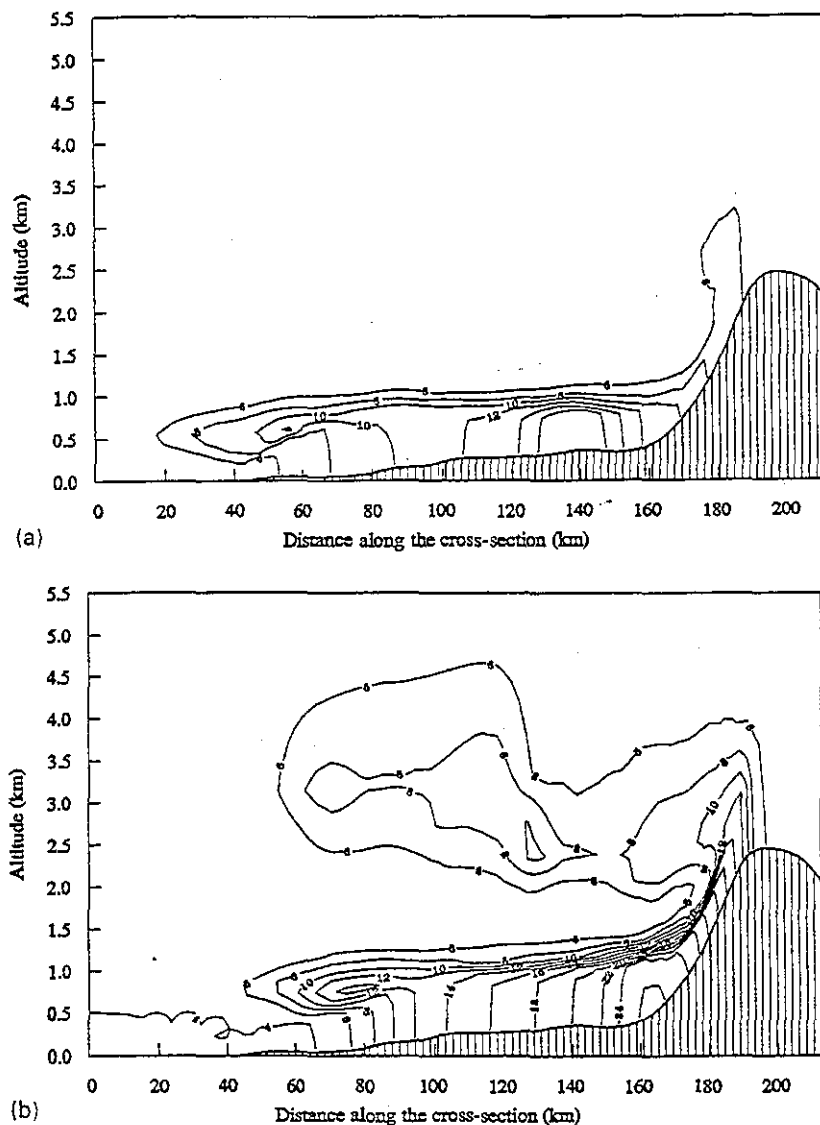


Fig. 11. Predicted ozone concentrations (contours, in intervals of 2 ppb) in vertical cross-section EE' (Fig. 1) bisecting the Los Angeles basin from Santa Monica Bay to the San Bernardino Mountains, on 27 August 1987. (a) 12:00 PST; (b) 16:00 PST; (c) 20:00 PST.

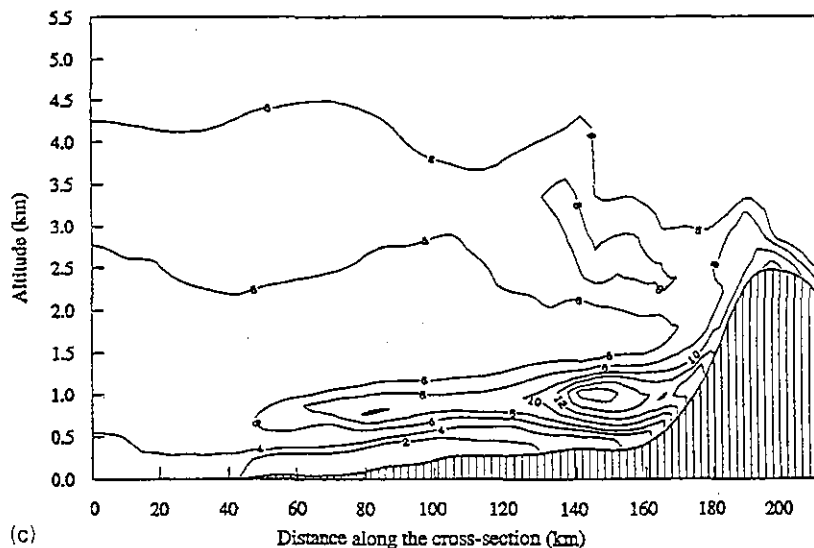


Fig. 11c.

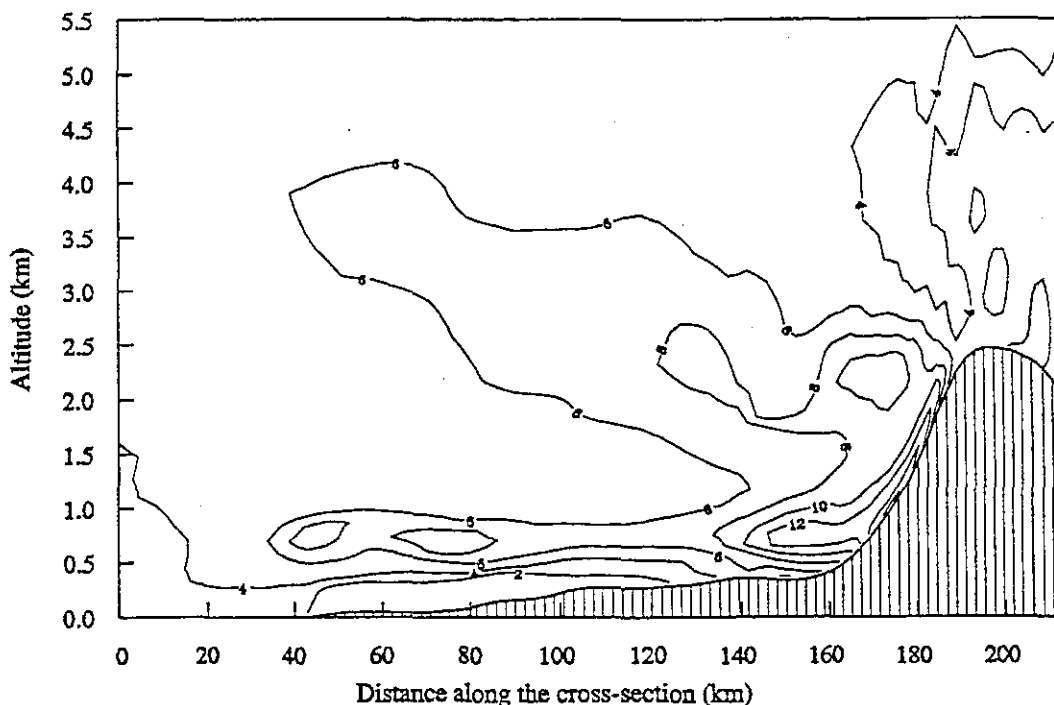


Fig. 12 Simulated ozone concentrations (contours, in intervals of 2 pphmv) in vertical cross-section EE' (Fig. 1) (from Santa Monica Bay to the San Bernardino Mountains) at 20:00 PST on 28 August 1987.

concentrations at ground level. The three-dimensional ozone distributions described above point to the origins of variations in surface ozone abundances around the Los Angeles basin. Early in the day, ground-level ozone concentrations are modulated by the depth of the boundary layer and induced sea breezes. In coastal regions, when marine air is flowing onshore, ozone concentrations are limited to about 10 pphmv or less. In general, afternoon surface ozone

concentrations increase steadily from the western coastal zone toward the eastern basin and inland mountains, as aged polluted air is drawn eastward by sea-breezes and mountain flow. Accordingly, the highest levels of ozone usually occur in the eastern basin and along the southern slopes of the San Gabriel Mountains.

During the evening, the stabilization of the mixed layer traps photochemically-aged pollutants in the

temperature inversion aloft, forming elevated layers with high concentrations of pollutants. Below these layers, relatively clean marine air pushes inland in the evening hours. Further, emissions of NO can reduce ozone concentrations near the surface by titration. Hence, nighttime surface ozone concentrations are generally low across the basin. Nevertheless, high concentrations of ozone are seen along mountain slopes that intersect elevated pollution layers. Nighttime drainage flows can also carry ozone back down the mountain slopes.

The following morning, polluted air in elevated layers can be entrained into the mixed layer as the boundary layer depth grows. This entrainment process can contribute to a rapid increase in surface ozone concentrations even when winds are stagnant, particularly in the eastern basin. The potential ozone source is quantified in Section 5.

4.3. Chemistry of pollution layers

The pollution layers stabilized within the temperature inversion are composed of photochemically-aged heavily contaminated air. Secondary pollutants comprise most of the trace components of these layers. Isolated from removal by dry deposition at the surface, pollutants in these elevated layers have a long lifetime; moreover, because mixing is suppressed at these heights, the residence time aloft is greatly enhanced. Thus, isolated from surface sources and deposition, photochemical processing can proceed to completion in these layers.

A variety of secondary pollutants are generated photochemically and accumulate in the polluted layers. Ozone and other oxidants are the most important of these compounds. Among the important secondary pollutants are peroxyacetyl nitrate (PAN), other organic nitrates, nitric acid (HNO_3), and a variety of oxidized hydrocarbons including acrolein. An example of the predicted vertical distribution of PAN is shown in Fig. 13. Note that, during the evening substantial quantities of PAN are found aloft; this material is not subject to surface removal. Like ozone, PAN and the other noxious photochemical byproducts in these layers can return to the surface the following day.

High concentrations of nitrate radicals (NO_3) and dinitrogen pentoxide (N_2O_5) are also found in the polluted layers at night. Isolated from surface emissions of NO and NMHCs, NO_3 is mainly converted into N_2O_5 . N_2O_5 in turn may undergo heterogeneous conversion to HNO_3 on aerosol surfaces, inasmuch as the polluted layers contain heavy loadings of particulates.

Low NO concentrations appear in the elevated layers where O_3 can maintain relatively high concentrations. This situation is quite different from conditions at the surface, where continuing NO emissions are trapped below the nocturnal temperature inversion, allowing nitric oxide and nitrogen dioxide concentrations build up near the surface at night. In this surface layer, ozone concentrations are characteristically low, owing in part to the titration reaction of NO with O_3 (although this reaction does not reduce

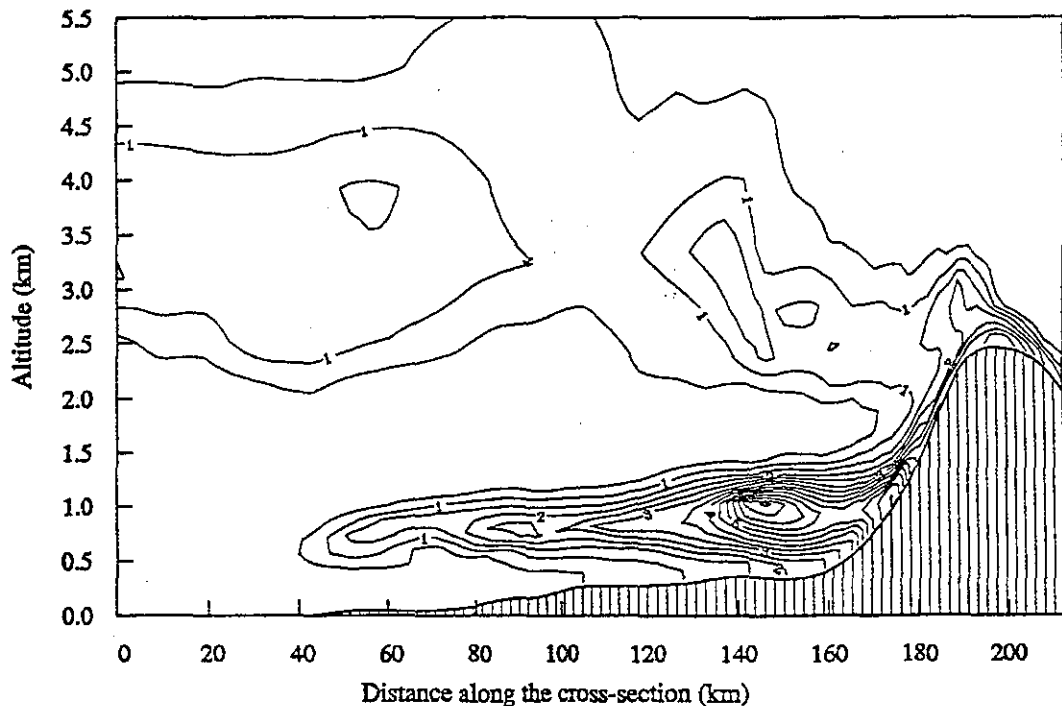


Fig. 13. Calculated PAN concentrations (contours, in intervals of 0.5 ppbv) for a vertical cross-section from Santa Monica Bay to the San Bernardino Mountains (EE' in Fig. 1) at 20:00 PST on 27 August 1987.

the total oxidant concentration). The titration reaction enhances the contrast in the concentration profile of O_3 (and NO) between the surface and the elevated layers.

Pollutants with relatively long lifetimes and dominant sources in emissions are expected to be found both in newly contaminated air and in aged polluted air. Carbon monoxide, for example, appears in elevated layers aloft and in air trapped near the surface in the evening (Fig. 14 shows a typical SMOG prediction for CO). The spatial distributions of such pollutants are more dependent on regional transport and dispersion, rather than on chemical transformations (except for possible minor secondary photochemical sources, as in the case of CO).

Since aerosols in polluted air are generated primarily by gas-to-particle conversion involving photochemical byproducts (particularly sulfates, nitrates and low-volatility organics), these aerosols are expected to have significant abundances in the polluted layers stabilized in the inversion aloft. In fact, dense aerosol layers have been observed over the Los Angeles basin by airborne lidar (e.g. Wakimoto and McElroy, 1986). These aerosol enhancements are coincident with the ozone layers described earlier.

5. POLLUTANT RECIRCULATION IN THE BASIN

Pollutants trapped in stabilized layers can be entrained downward into the boundary layer during the

morning hours as the mixed layer deepens with solar heating. To determine the potential impact of stabilized photochemically-aged air on surface ozone concentrations, the SMOG model was used to calculate the relative contributions of primary emissions and recirculated secondary pollutants during a 24 h period. Toward this end, two model runs were carried out for 27–28 August 1987. In the first simulation (case NE, no emissions), all surface emissions were terminated and initial pollutant distributions were equated to the predicted concentrations at 18:00 PST on 27 August, obtained from a continuous three-day simulation (described earlier). Therefore, case NE represents the impact of residual aged pollutants from the 27th on ozone abundances on the 28th. The second simulation (case NP, no initial pollutants) includes surface emissions, but assumes background species concentrations initially. In the absence of aged pollutants, case NP defines the pollutant concentrations generated on the 28th owing to the primary emissions during the 24 h period. Both the NE and NP simulations were initiated at 18:00 PST, at which time ozone photochemical production is negligible.

In case NE, ozone produced on the 27th is transported to and stored in stabilized layers during the evening. Some of this residual ozone (as well as other oxidants and secondary pollutants) is mixed downward on the following morning (the 28th). Figure 15 depicts the surface ozone concentrations predicted at 12:00 PST on 28 August for the case NE. The largest values are seen in the eastern basin and east of the

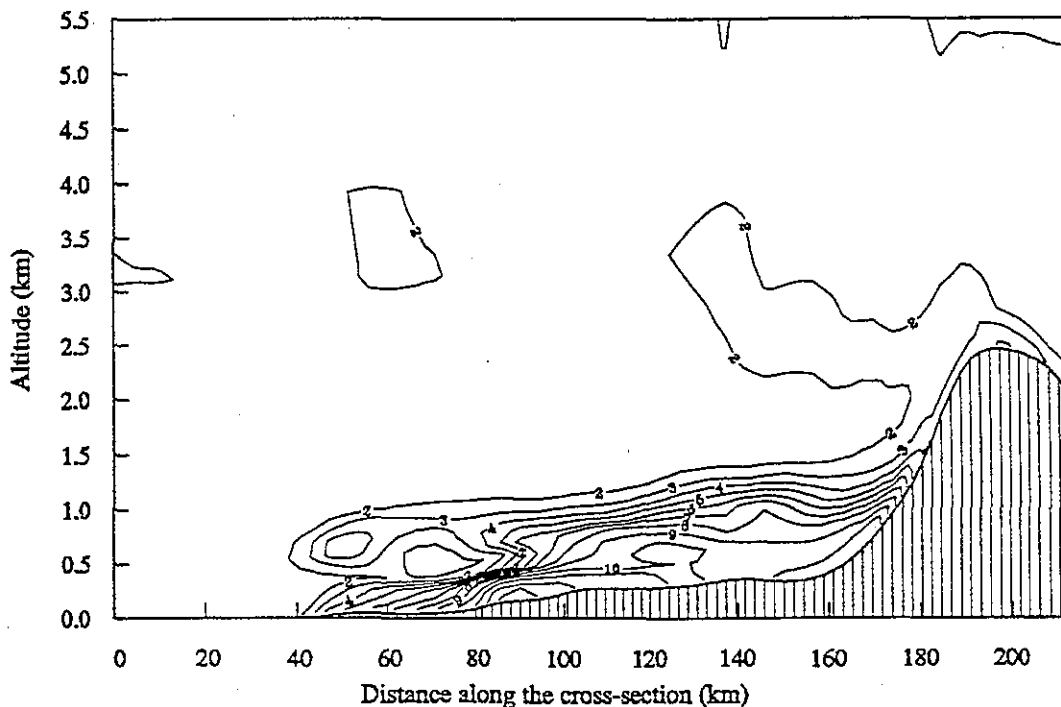


Fig. 14. Predicted CO concentrations (contours, in intervals of 0.1 ppmv) in vertical cross-section EE' (Fig. 1) (from Santa Monica Bay to the San Bernardino Mountains) at 20:00 PST on 27 August 1987.

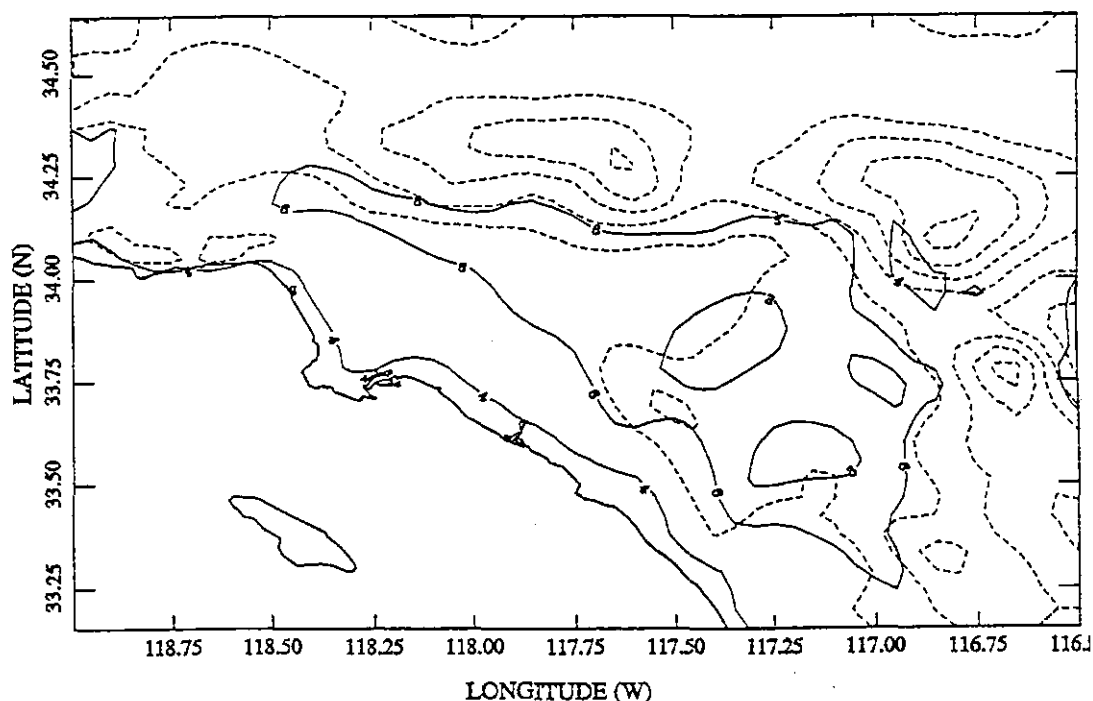


Fig. 15. Ozone mixing ratios near the surface at 12:00 PST on 28 August 1987 in a simulation in which all emissions of primary pollutants were suppressed on the 28th (case NE, see the text) but aged pollutants were present from the previous day. The ozone contour interval is 2 pphmv. Terrain features are shown as dashed lines.

Santa Ana mountains, where ozone levels of 6–8 pphmv occur. Ozone concentrations peak in the area east of the Santa Ana mountains. Over the western regions of the basin, away from the coastline, surface ozone abundances are in the range of 4–6 pphmv. The concentrations are moderated later in the afternoon as polluted air is gradually ventilated from the basin.

Another estimate of the surface effects of residual pollutants on the 28th can be obtained by subtracting the ozone concentrations predicted in case NP, which includes the effects of primary emissions but no aged pollutants, from the concentrations simulated in the continuous three-day run, which includes both effects. Figure 16 illustrates these surface ozone concentration differences at 12:00 PST on 28 August. Again, a peak abundance of above 8 pphmv is found in the eastern basin. The ozone concentration reaches a maximum value of about 6 pphmv at 14:00 PST, and decreases gradually later in the day. In the western basin, the contributions of stabilized layers to surface ozone are in the range of 2 pphmv. These amounts are somewhat smaller than those shown in Fig. 15 in part because ozone can be titrated by freshly emitted nitric oxide, which is absent in the case of NE.

Both of the simulations, NE and NP, clearly demonstrate the significance of pollutant recirculation in the Los Angeles basin. During the evening, substantial quantities of aged contaminated air are stabilized in elevated layers above the basin; these layers serve as a reservoir, and later a source, of secondary pollut-

ants. Downward-mixing the following day provides a mechanism for delivering the stored pollutants to the surface. This recycling process can explain the rapid increase in surface ozone concentrations frequently observed in the eastern regions of the Los Angeles basin during the morning hours. The contribution of recirculation to surface ozone concentrations is as great as 8 pphmv in the eastern regions.

6. SUMMARY AND DISCUSSION

An integrated air pollution modeling system (SMOG) has been used to investigate the relationships between meteorology, pollutant dispersion, and air quality in the Los Angeles basin (Lu, 1994; Lu *et al.*, 1995 a, b). In this work, the spatial and temporal distributions of ozone on 27 and 28 August 1987 have been simulated and analyzed in detail. The highly non-uniform surface ozone concentrations measured in the basin are a consequence of complex three-dimensional coupled dynamical/photochemical processes. The highest levels of ozone are predicted in the eastern basin and along the slopes of the surrounding mountain barriers, as observed. Moreover, SMOG simulations have revealed for the first time the role of stabilized layers of pollution, which are a common feature over Los Angeles, as an important secondary source of ground-level ozone and other pollutants, including PAN, nitric acid and organic nitrates.

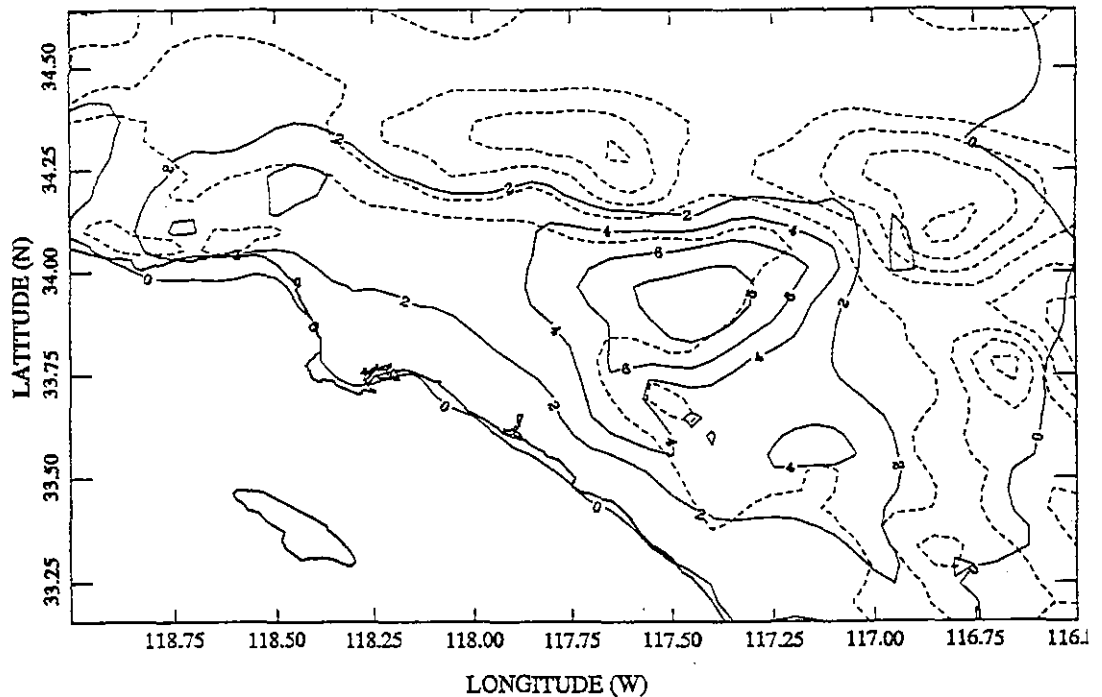


Fig. 16. Differences in ozone concentrations near the surface at 12:00 PST on 28 August 1987 between the standard three-day simulation and the simulation in which only one day's emissions and chemistry occur starting from background conditions (case NP). The ozone contour intervals are 2 pphmv.

The impact of photochemically-aged air from aloft on surface ozone concentrations is estimated to be as high as 8 pphmv in the eastern Los Angeles basin. In fact, rapid increases in surface ozone frequently noted in the eastern basin during the morning hours can be attributed to fumigation from stabilized layers of pollution. Vertical circulations associated with sea-breezes and mountain flows lead to the formation of these layers (Lu and Turco, 1994, 1995). High mountains surrounding the basin hinder long-range dispersion and confine pollutants within the basin. During the afternoon and evening, these accumulated materials are transported to and stabilized within the temperature inversion blanketing the region. The following day, secondary pollutants are mixed downward, enhancing surface concentrations. Accordingly, the mechanism of pollutant recirculation and surface enhancement in the Los Angeles basin is a fundamental consequence of meteorological conditions. It follows that other urban areas with similar terrain and climate should experience comparable effects.

The SMOG simulations also reveal the major pathways leading to the dispersion of pollutants from the Los Angeles basin. A "chimney" effect caused by upslope winds on heated mountain slopes vents pollutants directly into free troposphere during the afternoon. As a result, layers of pollution are created in the free troposphere, which contribute to regional and global scale dispersion of these materials. Also impor-

tant is the advection of contaminated air over major mountain passes bisecting the ranges surrounding Los Angeles. In the late afternoon, pollutants are effectively transported across the mountains, particularly through the Cajon and Newhall passes. Consequently, pollutants are carried to the high desert region where air quality and visibility can be significantly degraded.

An obvious conclusion of this work is the need for validated three-dimensional coupled meteorological/chemical models of urban air sheds. Our simulations and analyses have demonstrated the importance of explicitly resolving the dynamics of the boundary layer, the coupling between the mixed layer and free troposphere, and the interactions of air flow with terrain in complex coastal settings. With a modeling system like SMOG, the formation of stabilized layers of polluted air and the recirculation of secondary pollutants can be studied and understood (Lu, 1994; Lu *et al.*, 1995a). Moreover, the competing modes of regional and long-range transport of pollutants can be quantified. In this regard, model predictions are helpful in pointing to essential field measurements and monitoring activities that can lead to a better characterization of air pollution. Finally, any attempts to develop policies for controlling primary emissions and improving air quality using numerical predictions must be based on reliable scientifically-validated models. The capability of air quality models

in simulating pollutant levels aloft is an important aspect in evaluating the performances of air quality models.

Acknowledgements—This paper is based on Chap. 10 of Rong Lu's Ph.D. dissertation. The computations were performed at the NASA Ames Research Center National Aeronautics Simulation facility (project NAS-802) and the EPA National Environmental Supercomputer Center. The work reported here was partially supported by the National Science Foundation under grant ATM-92-16646 and Environmental Protection Agency under grant CR-823755-01.

REFERENCES

- Allen P. D. and Wagner K. K. (1992) 1987 SCAQS emission inventory, magnetic tape numbers ARA806 and ARA807. Technical Support Division, California Air Resources Board, Sacramento, California.
- Anderson J. A., Koos J. C. and Hammarstrand R. G. M. (1989) Summary of SCAQS upper air measurements performed by the STI aircraft. Report No. 97010-902FR, prepared for the California Air Resources Board Contract No. A6-098-32, Sonoma Technology, Inc., Santa Rosa, California.
- Blumenthal D. L., White W. H. and Smith T. B. (1978) Anatomy of a Los Angeles smog episode: pollutant transport in the daytime sea breeze regime. *Atmospheric Environment* 12, 893-907.
- Cassmassi J. C. and Durkee K. R. (1990) Comparison of mixing height fields for UAM application generated from limited and multiple temperature sounding profiles in the South Coast Air Basin. A&WMA Specialty Conference on Tropospheric Ozone and the environment, 20-22 March 1990, Industry Hills, California.
- Edinger J. G. (1973) Vertical distribution of photochemical smog in Los Angeles basin. *Envir. Sci. Technol.* 7, 247-252.
- Edinger J. G., McCutchan M. H., Miller P. R., Ryan B. C., Schroeder M. J. and Behar J. V. (1972) Penetration and duration of oxidant air pollution in the south coast air basin of California. *J. Air Pollut. Control Ass.* 22, 882-886.
- Fujita E. M., Croes B. E., Bennett C. L., Lawson D. R., Lurmann F. W. and Main H. H. (1992) Comparison of emission inventory and ambient concentration ratios of CO, NMHC, and NO_x in California's south coast air basin. *J. Air Waste Man. Ass.* 42, 264-276.
- Gear C. W. (1969) The automatic integration of stiff ordinary differential equations. In *Information Processing* (edited by Morrel A. J. H.), Vol. 68, pp. 187-193. North-Holland, Amsterdam.
- Gear C. W. (1971) *Numerical Initial Value Problems in Ordinary Differential Equations*, 253 pp. Prentice-Hall, Englewood Cliffs, N.J.
- Gery M. W., Whitten G. Z., Killus J. P. and Dodge M. C. (1989) A photochemical kinetics mechanism for urban and regional scale computer modeling. *J. geophys. Res.* 94, 12,925-12,956.
- Harley R. A., Russell A. G., McRae G. J., Cass G. R. and Seinfeld J. H. (1993) Photochemical modeling of the Southern California Air Quality Study. *Envir. Sci. Technol.* 27, 378-388.
- Ingalls M. N., Smith L. R. and Kirksey R. E. (1989) Measurement of on-road vehicle emission factors in the California South Coast Air Basin — Vol. I: Regulated emissions. Report No. SwRI-1604 from the southwest Research Institute to the Coordinating Research Council, Atlanta, Georgia.
- Jacobson M. Z. (1994) Developing, coupling, and applying a gas, aerosol, transport, and radiation model to study urban and regional air pollution. Ph.D. thesis, Dept. of Atmospheric Sciences, Univ. California, Los Angeles, California.
- Jacobson M. Z. and Turco R. P. (1994) SMVGEAR: A sparse-matrix, vectorized Gear code for atmospheric models. *Atmospheric Environment* 28A, 273-284.
- Jacobson M. Z., Lu R., Turco R. P. and Toon O. B. (1995) Development and application of a new air pollution model system. Part I: Gas-phase simulations. *Atmospheric Environment* 30B, 1939-1963.
- Lu R. (1988) The design and development of a three-dimensional fine-mesh limited area model for typhoon and mesoscale system prediction. M.S. thesis, Nanjing Univ., Nanjing, China.
- Lu R. (1994) Development of an integrated air pollution modeling system and simulations of ozone distributions over the Los Angeles basin. Ph.D. dissertation, Univ. California, Los Angeles.
- Lu R. and Cheng Z. (1989) A preliminary forecasting test for the six-layer fine-mesh mesoscale numerical model. *J. Nanjing Inst. Met.* 12, 81-86.
- Lu R. and Turco R. P. (1994) Air pollution transport in a coastal environment: Part I: two-dimensional simulation of sea-breeze and mountain effects. *J. Atmos. Sci.* 51, 2285-2308.
- Lu R. and Turco R. P. (1995) Air pollution transport in a coastal environment: Part II: three-dimensional simulations over the Los Angeles basin. *Atmospheric Environment* 29B, 1499-1518.
- Lu R., Turco R. P. and Jacobson M. (1995a) An integrated air pollution modeling system for urban and regional scales. Part I: structure and performance. *J. geophys. Res.* (to appear).
- Lu R., Turco R. P. and Jacobson M. (1995b) An integrated air pollution modeling system for urban and regional scales. Part II: simulations for SCAQS 1987. *J. geophys. Res.* (to appear).
- McElroy J. L. (1982) Investigation of episodic air quality using airborne lidar. *Proc. Third Joint Conf. on Applications of Air Pollution Meteorology*, San Antonio, Amer. Meteor. Soc., pp. 143-148.
- McElroy J. L. and Smith T. B. (1986) Vertical pollutant distributions and boundary layer structure observed by airborne lidar near the complex southern California coastline. *Atmospheric Environment* 20, 1555-1566.
- McElroy J. L. and Smith T. B. (1991) Lidar descriptions of the mixing-layer thickness characteristics in a complex terrain/coastal environment. *J. appl. Met.* 30, 585-597.
- McElroy J. L. and Smith T. B. (1992) Creation and fate of ozone layers aloft in Southern California. *Atmospheric Environment* 26, 1917-1929.
- McRae G., Goodin W. R. and Seinfeld J. (1982a) Mathematical modeling of photochemical air pollution. California Air Resources Board, Nos. A5-046-87 and A7-187-30.
- McRae G., Goodin W. R. and Seinfeld J. (1982b) Development of a second-generation mathematical model for urban air pollution I. Model formulation. *Atmospheric Environment* 16, 679-696.
- Malone R. C., Auer L. H., Glatzmaier G. A., Wood M. C. and Toon O. B. (1986) Nuclear winter: Three-dimensional simulations including interactive transport, scavenging and solar heating of smoke. *J. geophys. Res.* 91, 1039-1054.
- Pierson W. R., Robinson N. F. and Gertler A. W. (1992) Review and reconciliation of on-road emission factors in the SoCAB, Southern California Air Quality Study Data Analysis, Proc. Int. Specialty Conf., July 1992, Los Angeles, California, pp. 35-42.
- Roberts P. and Main H. (1992) Analysis of 3D air quality data and carbon, nitrogen, and sulfur species distributions during the Southern California Air Quality Study. Final report. Prepared for Coordinating Research Council under contract No. SCAQS-8-4.

- Russell A. G., McCue K. F. and Cass G. R. (1988) Mathematical modeling of the formation of nitrogen-containing air pollutants. 1. Evaluation of an Eulerian photochemical model. *Envir. Sci. Technol.* **22**, 263-271.
- SCAQMD (1990) Draft AQMP 1991 Revision Technical Report V-B Ozone Modeling—Performance Evaluation, December. [Available from South Coast Air Quality Management District, Diamond Bar, California.]
- SCAQMD (1991) Final AQMP 1991 Revision Technical Report V-B Ozone Modeling—Performance Evaluation, July. [Available from South Coast Air Quality Management District, Diamond Bar, California.]
- Scheffe R. D., Morris R. E. (1993) A review of the development and application of the urban airshed model. *Atmospheric Environment* **27B**, 23-39.
- Schultz P. and Warner T. T. (1982) Characteristics of summertime circulations and pollutant ventilation in the Los Angeles Basin. *J. appl. Met.* **21**, 672-682.
- Smith T. B. and Edinger J. G. (1984) Utilization of remote sensing data in the evaluation of air pollution characteristics in the south coast/southeast desert air basin. California Air Resources Board, No. A2-106-32.
- Toon O. B. and Ackerman T. P. (1981) Algorithms for the calculation of scattering by stratified spheres. *Appl. Opt.* **20**, 3657-3660.
- Toon O. B., Turco R. P., Hamill P., Kiang C. S. and Whitten R. C. (1979) A one-dimensional model describing aerosol formation and evolution in the stratosphere. Part II. Sensitivity studies and comparison with observations. *J. Atmos. Sci.* **36**, 718-736.
- Toon O. B., Kasting J. F., Turco R. P. and Liu M. S. (1987) The sulfur cycle in the marine atmosphere. *J. geophys. Res.* **92**, 943-963.
- Toon O. B., Turco R. P., Westphal D., Malone R. and Liu M. S. (1988) A multidimensional model for aerosols: Description of computational analogs. *J. Atmos. Sci.* **45**, 2123-2143.
- Toon O. B., Turco R. P., Jordan J., Goodman J. and Ferry G. (1989a) Physical processes in polar stratospheric ice clouds. *J. geophys. Res.* **94**, 11,359-11,380.
- Toon O. B., McKay C. P. and Ackerman T. P. (1989b) Rapid calculation of radiative heating rates and photodissociation rates in inhomogeneous multiple scattering atmospheres. *J. geophys. Res.* **94**, 16,287-16,301.
- Turco R. P. and Whitten R. C. (1977) The NASA Ames research center one and two dimensional stratospheric models Part I: The one dimensional model. NASA Tech. Publ. (TP) 1002.
- Turco R. P., Hamill P., Toon O. B., Whitten R. C. and Kiang C. S. (1979a) A one-dimensional model describing aerosol formation and evolution in the stratosphere. Part I: Physical processes and mathematical analogs. *J. Atmos. Sci.* **36**, 699-717.
- Turco R. P., Hamill P., Toon O. B., Whitten R. C. and Kiang C. S. (1979b) The NASA-Ames research center stratospheric aerosol model. I: Physical processes and Computational analogs. NASA TECH. Publ. (TP) 1362, iii-94.
- Turco R. P., Toon O. B. and Whitten R. C. (1982a) Stratospheric aerosols: Observation and theory. *Rev. Geophys. Space Phys.* **20**, 233-279.
- Turco R. P., Toon O. B., Whitten R. C., Keesee R. G. and Hamill P. (1982b) Importance of heterogeneous processes to tropospheric chemistry: Studies with a one-dimensional model. *Heterogeneous Atmos. Chem. Geophys. Monograph Series* **26**, 231-240.
- Ulrickson B. L. and Mass C. F. (1990a) Numerical investigation of mesoscale circulations over the Los Angeles basin. Part I: A verification study. *Mon. Weath. Rev.* **118**, 2162-2184.
- Ulrickson B. L. and Mass C. F. (1990b) Numerical investigation of mesoscale circulations over the Los Angeles basin. Part II: Synoptic influences and pollutant transport. *Mon. Weath. Rev.* **118**, 2162-2184.
- Wagner K. K., Wheeler N. J. M. and McNerny D. L. (1992) The effect of emission inventory uncertainty on Urban Airshed Model sensitivity to emission reductions. Tropospheric Ozone: Non-attainment and Design Value Issues. In *Proc. Int. Specialty Conf.* (edited by Vostal J. J.), pp. 123-134. A&WMA Transaction Series No. 23, Pittsburgh, PA.
- Wakimoto R. M. and McElroy J. L. (1986) Lidar observation of elevated pollution layers over Los Angeles. *J. Clim. appl. Met.* **25**, 1583-1599.
- Westphal D. L. and Toon O. B. (1991) Simulations of microphysical, radiative, and dynamical processes in a continental-scale forest fire smoke plume. *J. geophys. Res.* **96**, 22,379-22,400.
- Westphal D. L., Toon O. B. and Carlson T. N. (1988) A case study of transport and mobilization of Saharan dust storms. *J. Atmos. Sci.* **45**, 2144-2160.